JOURNAL OF PETROLOGY | VOLUME 45 | NUMBER 9 | PAGES 1821–1844 | 2004 | DOI: 10.1093/petrology/egh035

Ultrahigh-temperature Metamorphism (1150°C, 12 kbar) and Multistage Evolution of Mg-, Al-rich Granulites from the Central Highland Complex, Sri Lanka

K. SAJEEV[1]* AND Y. OSANAI[2]

[1]DEPARTMENT OF EARTH AND PLANETARY SYSTEM SCIENCES, OKAYAMA UNIVERSITY, TSUSHIMA NAKA 3-1-1, OKAYAMA, JAPAN

[2]DIVISION OF EVOLUTION OF EARTH ENVIRONMENTS, GRADUATE SCHOOL OF SOCIAL AND CULTURAL STUDIES, KYUSHU UNIVERSITY, ROPPONMATSU, FUKUOKA 810-8560, JAPAN

RECEIVED MARCH 22, 2003; ACCEPTED MARCH 30, 2004
ADVANCE ACCESS PUBLICATION JULY 22, 2004

Mg- and Al-rich granulites of the central Highland Complex, Sri Lanka preserve a range of reaction textures indicative of a multistage P–T *history following an ultrahigh-temperature metamorphic peak. The granulites contain a near-peak assemblage of sapphirine–garnet–orthopyroxene–sillimanite–quartz–K-feldspar, which was later overprinted by intergrowth, symplectite and corona textures involving orthopyroxene, sapphirine, cordierite and spinel. Biotite-rims, kornerupine and orthopyroxene-rims on biotite are considered to be late assemblages. Thermobarometric calculations yield an estimated* P–T *of at least 1100°C and 12 kbar for the near-peak metamorphism. Isopleths of Al_2O_3 in orthopyroxene are consistent with a peak temperature above 1150°C. The* P–T *path consists of four segments. Initial isobaric cooling after peak metamorphism (Segment A), which produced the garnet–sapphirine–quartz assemblage, was followed by near-isothermal decompression at ultrahigh temperature (Segment B), which produced the multiphase symplectites. Further isobaric cooling (Segment C) resulted in the formation of biotite and kornerupine, and late isothermal decompression (Segment D) formed orthopyroxene rims on biotite. This evolution can be correlated with similar* P–T *paths elsewhere, but there are not yet sufficient geochronological and structural data available from the Highland Complex to allow the tectonic implications to be fully assessed.*

KEY WORDS: *central Highland Complex; granulites; multistage evolution; Sri Lanka; UHT metamorphism*

INTRODUCTION

Textural interpretation of mineral assemblages is integral to understanding ultrahigh-temperature (UHT) metamorphism in granulites. Extremely high Al- and Mg-granulites commonly preserve near-peak assemblages and a range of related reaction textures that are a direct record of their *P–T* evolution (Hensen, 1987).

Based on Nd-model age mapping by Milisenda *et al.* (1988) and geochronological work by Kröner *et al.* (1991), the supracrustal rocks of Sri Lanka have been subdivided into four major terranes: the Wanni, Kadugannawa, Highland and Vijayan Complexes (Fig. 1). The highest-grade metamorphic rocks are in the Highland Complex, which can be subdivided into the western, eastern and southwestern Highland Complexes, based on model ages (Milisenda *et al.*, 1988) and metamorphic grade (e.g. Sajeev, 2003). Some workers consider the western Highland Complex to be part of the eastern and south-western Highland Complexes because of the range of model ages (Fig. 1), and some consider the western Highland Complex to be part of the Wanni Complex.

The Highland Complex (Fig. 2) consists of aluminous migmatitic gneisses, intercalated with mafic granulites, calc-silicate gneisses and orthopyroxene-bearing granitic rocks (charnockite). Petrological studies of the pelitic granulites reveal that most of this vast terrane evolved along a clockwise *P–T* path at medium to high pressure

*Corresponding author. Present address: Basic Science Research Institute, Chonbuk National University, Chonju 561-756, South Korea. Telephone: (+82)-63-270-3397, Fax: (+82) 63-270-3399.
E-mail: sajeev@chonbuk.ac.kr

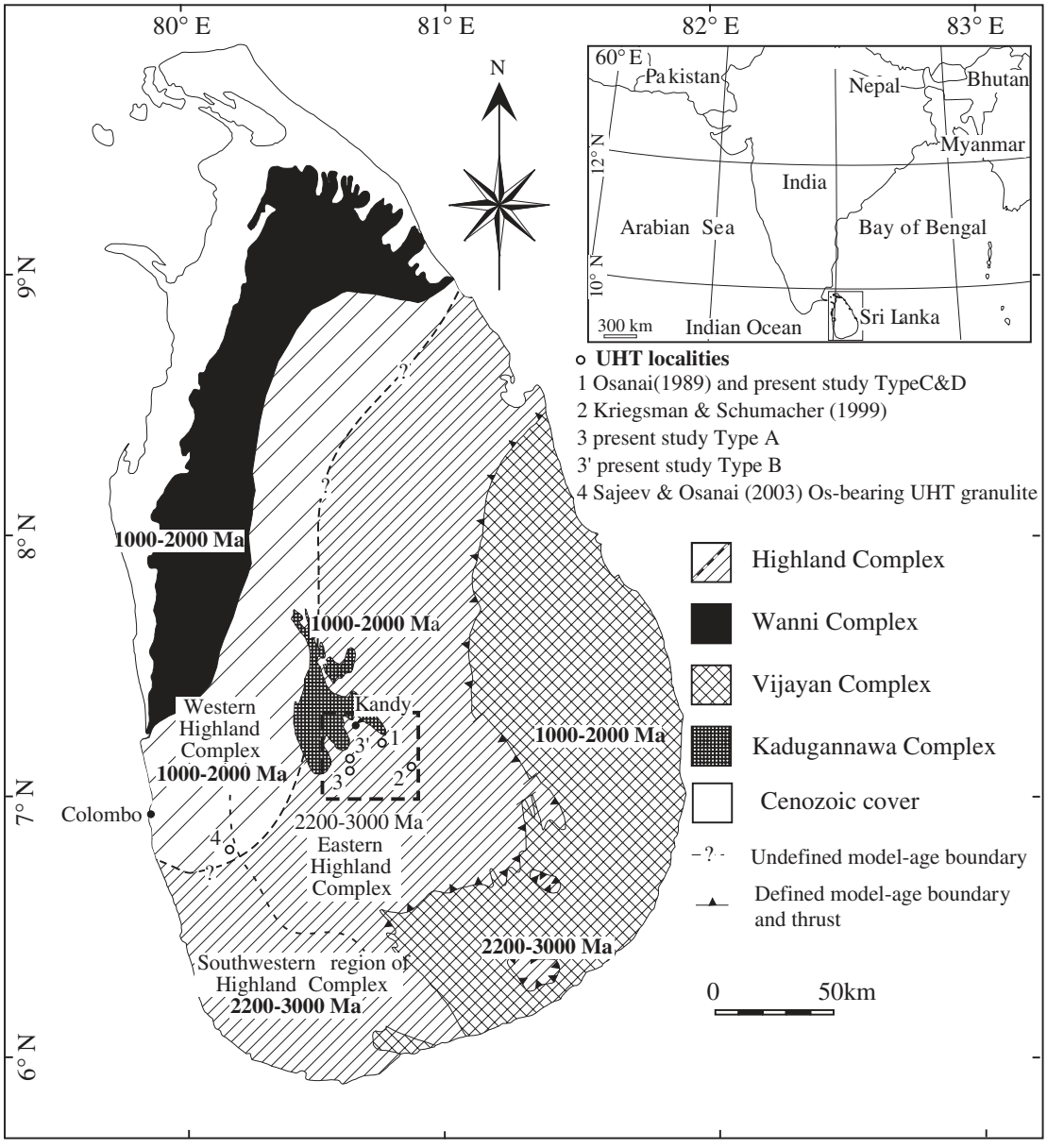

Fig. 1. Tectonic classification of Sri Lankan geology. Modified after Kriegsman (1991a) and Schumacher & Faulhaber (1994). Boundaries and model ages are after Milisenda *et al.* (1988). Dashed box represents the area of Fig. 2.

and temperature (e.g. Prame, 1991; Hiroi *et al.*, 1994; Raase & Schenk, 1994). The first evidence for the prograde part of this path was reported by Hiroi *et al.* (1994).

The grade of metamorphism is highest in the central Highland Complex, where Osanai (1989) first reported sapphirine-bearing granulites. Other high-grade assemblages have subsequently been described by Kriegsman (1991*b*), Kriegsman & Schumacher (1999), Osanai *et al.* (2000, 2003) and Sajeev & Osanai (2002, 2003). Kriegsman & Schumacher (1999) and Osanai *et al.* (2000) first showed that the UHT metamorphism of the sapphirine-bearing granulites also followed a clockwise *P–T* path. Schenk *et al.* (1988) reported temperatures above 900°C for mafic granulites from the central Highland Complex based on orthopyroxene exsolution in clinopyroxene, which they interpreted as evidence for isobaric cooling from even higher temperatures. Sajeev & Osanai (2002) argued that the post-peak cooling of the sapphirine–quartz assemblage was isobaric.

In this paper, we discuss the petrography, textural relationships and mineral chemistry of a suite of UHT high Mg- and Al-granulites from the central Highland Complex that preserves evidence for several distinct

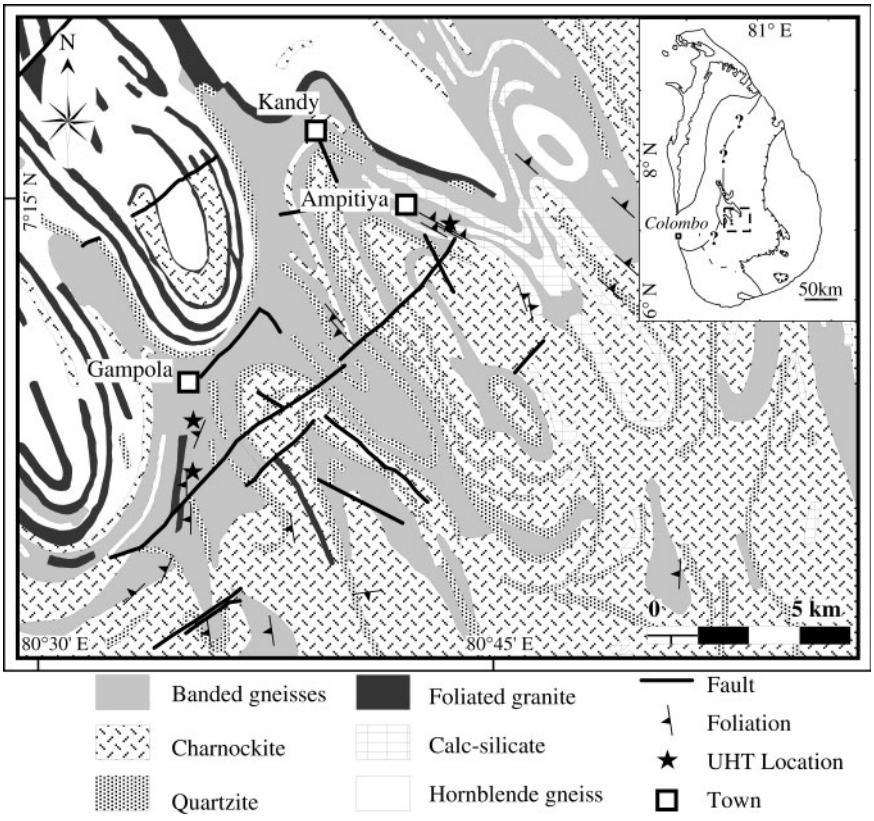

Fig. 2. Geological map of the central Highland Complex, modified from the map by the Geological Survey Department of Sri Lanka (1982).

stages of evolution after the metamorphic peak. The rocks described were collected from three different localities and include garnet–sapphirine–orthopyroxene–quartz–sillimanite granulite (3107B), garnet-bearing orthopyroxene–sillimanite granulite (0101H), garnet–sapphirine–orthopyroxene granulite (0505E) and sapphirine–orthopyroxene–cordierite granulite (0505A).

FIELD RELATIONS

Garnet–sapphirine–orthopyroxene–quartz–sillimanite granulites were collected from a roadside exposure, south of Gampola (Fig. 3a and b), where they occur inter-layered with garnet–cordierite–biotite gneiss, two-pyroxene granulite and garnet–biotite gneiss. The dip of the foliation throughout the exposure is 50° to 265°.

Garnet-bearing orthopyroxene–sillimanite granulite is exposed in a quarry on the roadside near Kotmale Reservoir, south of Gampola. The exposure consists of disrupted mafic granulites and charnockites within migmatites. The granulite occurs in thin layers, including porphyroblasts of garnet, surrounded by macroscopic sillimanite, orthopyroxene and cordierite. Porphyroblasts of orthopyroxene associated with sillimanite can also be found (Fig. 3c). The general foliation dips 38° to 265°.

Garnet–sapphirine–orthopyroxene (Fig. 3d and e) and sapphirine–orthopyroxene–cordierite granulites (Fig. 3f) are exposed in a marble quarry at Talatuoya, near Ampitiya. The granulites occur as blocks within the marble, which is almost pure, containing only minor corundum, spinel and phlogopite. The garnet-free sapphirine–orthopyroxene–cordierite granulites are finer-grained and less common than the garnet–sapphirine–orthopyroxene granulite. Blocks of mafic granulite (up to 1 m in diameter) are also exposed.

MINERAL ASSEMBLAGES AND TEXTURAL RELATIONSHIPS

Samples from the three locations have been studied petrographically. All those from Gampola contain garnet porphyroblasts, 1–3 cm in diameter. In sample 3107B, sapphirine and quartz occur as inclusions in the garnet cores (Fig. 4a–c), but the inclusions in the garnet rims are orthopyroxene, sillimanite and quartz (Fig. 4d). Porphyroblasts of orthopyroxene are also present (Fig. 4e). In sample 0101H, the major inclusion phases in garnet are sillimanite and biotite. Some garnet cores also contain minor inclusions of oxide phases and spinel. None of the samples contains coexisting spinel and quartz. The

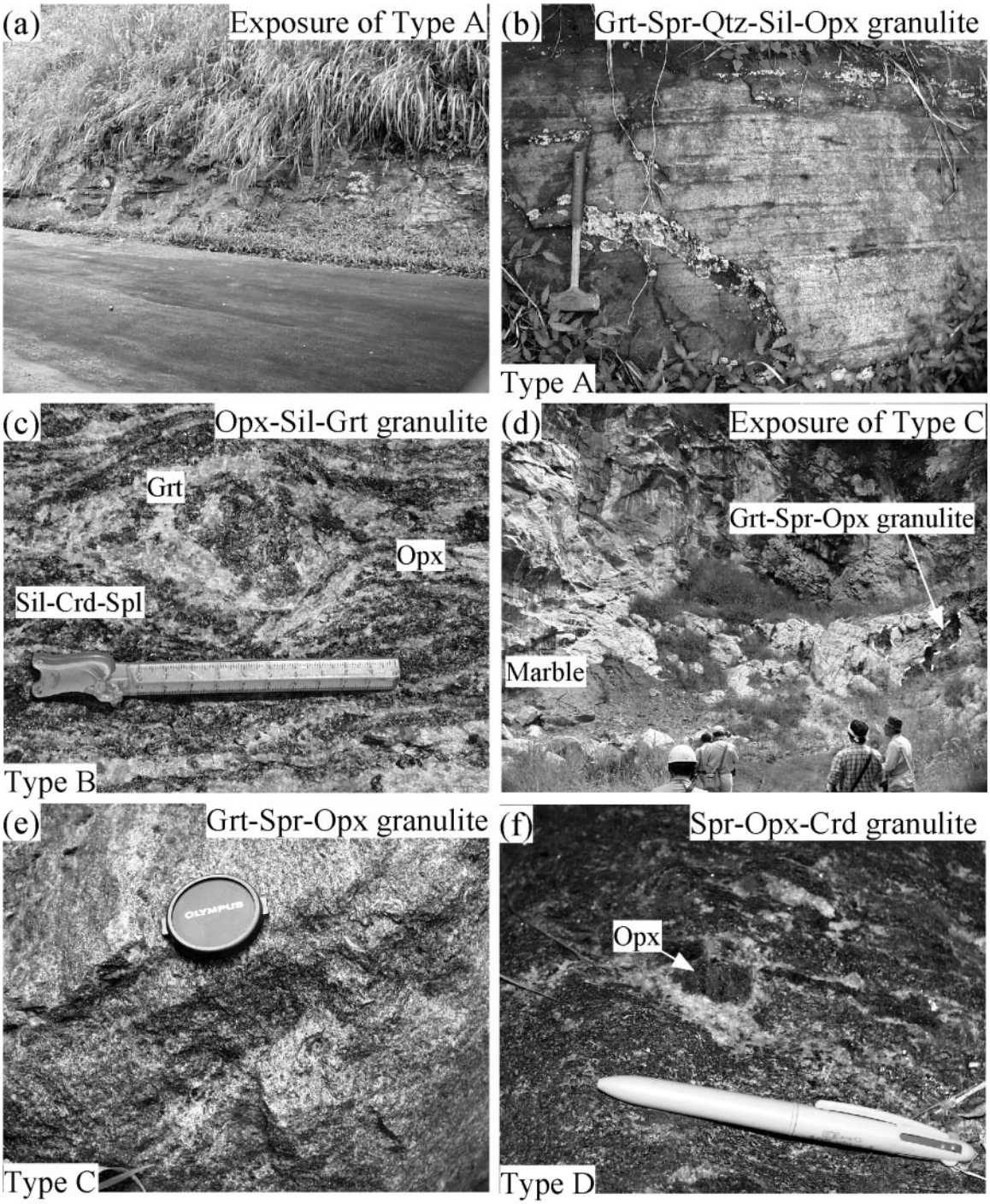

Fig. 3. (a) Roadside exposure of Type A samples near Gampola. (b) A close-up view of thin foliated gneisses from Type A exposure. (c) A close-up view of Type B sample. (Note the garnet rimmed by orthopyroxene–sillimanite–cordierite assemblage.) (d) The exposure of garnet–sapphirine–orthopyroxene granulite block (Type C) within the marble from Ampitiya. (e) A close-up view of Type C sample exposure. (f) Occurrence of Type D rock type.

samples from Talatuoya (0505A and 0505E) are mostly rich in orthopyroxene–sapphirine symplectites, with or without fine-grained (<1 mm) garnet. Quartz and sillimanite are absent (0505A and 0505E). Biotite is present in all the samples studied, but kornerupine was found only where garnet, quartz and sillimanite were absent.

The rocks thereby can be classified into four types: Type A (quartz and sillimanite present), Type B (quartz

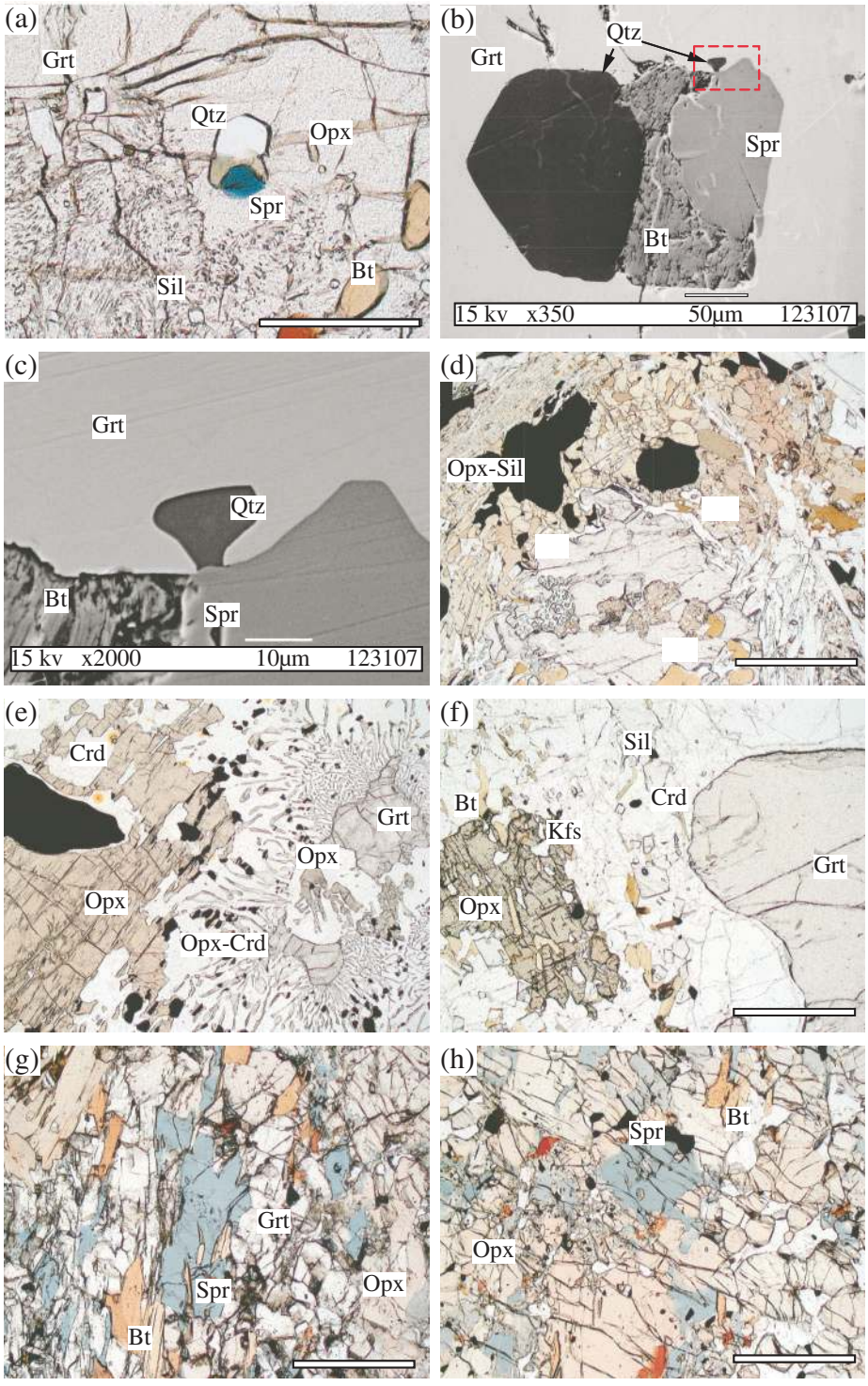

Fig. 4. Photomicrographs showing near-peak assemblages preserved in all four rock types. (a) Sapphirine–quartz inclusion in garnet porphyroblast. (b) Back-scattered electron image (BSI) of sapphirine–quartz coexistence inclusion in garnet. The square indicates the area of (c). (c) Enlarged BSI showing sapphirine–quartz direct coexistence. (d) Orthopyroxene porphyroblast and resorbed garnet separated by later cordierite-bearing assemblage in Type A sample. (e) Orthopyroxene–sillimanite–quartz with minor cordierite inclusion in garnet rims. (Note the associated orthopyroxene–sillimanite assemblage in the matrix.) (f) Garnet–orthopyroxene–K-feldspar ± cordierite porphyroblasts present as the near-peak assemblage identified from Type B samples. (g) Garnet, orthopyroxene, sapphirine ± biotite porphyroblasts in association present in Type C samples. (h) Orthopyroxene and sapphirine porphyroblasts from Type D samples. The scale bar for (a) represents 0·5 mm, while those for (d)–(h) represent 1 mm. The scale bar for back-scattered images in (b) represents 50 µm and that in (c) 10 µm.

Table 1: Mineral assemblages and textural features in UHT granulites of the central Highland Complex, Sri Lanka

Sample and position	Grt	Sil	Opx	Crd	Spr	Qtz	Pl	Kfs	Bt	Krn	Spl
Type A, 3107B											
Porphyroblast	C	C	C	C	—	I	I,N	I,N	I	—	I
Inclusion	—	B	B	—	A	A	—	—	O	—	—
Symplectite	—	D	D,G	G,L	—	D	—	—	L	—	G
Moat	—	—	—	J	—	—	—	—	—	—	—
Rim	—	—	M	M	—	—	—	M	K	—	—
Type B, 0101H											
Porphyroblast	C	C	C	—	—	—	I,N	N	I	—	I
Inclusion	—	—	—	—	—	—	—	—	O	—	—
Symplectite	—	E	E,G	G,L	—	—	—	—	L	—	—
Moat	—	—	—	J	—	—	—	—	—	—	—
Rim	—	—	—	—	—	—	—	—	K	—	—
Type C, 0505E											
Porphyroblast	C,I	—	C	—	C	—	I	—	I	—	—
Inclusion	—	—	—	—	—	—	—	—	O	—	—
Symplectite	—	—	G,H	F,G	F,H	—	—	—	—	—	G,H
Moat	—	—	—	J	—	—	—	—	—	—	—
Rim	—	—	—	—	—	—	—	—	K	—	—
Type D, 0505A											
Porphyroblast	—	—	C	—	C	—	I	—	I	I	—
Inclusion	—	—	—	—	—	—	—	—	O	—	—
Symplectite	—	—	G,H	F,G,L	F,H	—	—	—	L	—	—
Moat	—	—	—	J	—	—	—	—	—	—	—
Rim	—	—	—	—	—	—	—	—	K	—	—

Type A: quartz- and sillimanite-present samples. Type B: quartz-absent and sillimanite-present samples. Type C: quartz- and sillimanite-absent samples. Type D: quartz-, sillimanite- and garnet-absent samples.
A: Spr—Qtz inclusion in Grt; B: Opx—Sil—Qtz inclusion in Grt; C: porphyroblasts; D: Opx—Sil—Qtz intergrowth; E: Opx—Sil intergrowth; F: Spr—Crd symplectite; G: Opx—Crd—Spl symplectite; H: Spr—Opx/Opx—Spl symplectite; I: grain in the matrix/lobate; J: Crd moat on other mafic phases; K: Bt-rim on other mafic phases; L: Bt—Crd intergrowth; M: late Opx-rim on Bt; N: exsolution in feldspars; O: Bt inclusions.

absent, sillimanite present), Type C (quartz and sillimanite absent) and Type D (garnet, quartz and sillimanite absent). A summary of the mineral assemblages, mineral textures and textural relationships is given in Table 1.

Peak metamorphic assemblages (inclusions and porphyroblasts)

The peak mineral assemblages, as inferred from the inclusions and porphyroblast textures, differ between rock types. Relict garnet grains within the orthopyroxene–sapphirine symplectites in the Type C rocks are also considered to be primary. The peak mineral assemblages are interpreted to be as follows:

Type A (e.g. 3107B). Quartz and sillimanite plus sapphirine, garnet and orthopyroxene. Orthopyroxene–sillimanite–quartz inclusions in garnet rims might also be primary (Fig. 4d).

Type B (e.g. 0101H). Sillimanite plus garnet, orthopyroxene and K-feldspar (Fig. 4f).

Type C (e.g. 0505E). Garnet, orthopyroxene and sapphirine ± biotite (Fig. 4g). Garnet normally occurs as fine-grained relicts within symplectites, and orthopyroxene and sapphirine as coarse-grained porphyroblasts.

Type D (e.g. 0505A). Orthopyroxene and sapphirine ± biotite (Fig. 4h). The significance of the presence or absence of biotite inclusions to the peak assemblage is not yet clear.

Breakdown assemblages (symplectites, intergrowths, rims and moats)

Breakdown assemblages or reaction textures in the granulites consist mainly of symplectites, intergrowths, rims and moats. The principal mineral in these textures is

orthopyroxene, which forms various intergrowths and symplectites with other phases. Other minerals forming retrograde textures include cordierite, sapphirine, sillimanite and spinel. Biotite and kornerupine appear to be secondary. In some localized domains within quartz-bearing granulite, the biotite has a late rim of orthopyroxene. The principal retrograde reaction textures are as follows.

Orthopyroxene–sillimanite–quartz intergrowths

Medium to coarse intergrowths of orthopyroxene and sillimanite associated with fine- to medium-grained quartz are one of the dominant features of the Type A granulites (Fig. 5a). In some domains, grain boundaries of orthopyroxene–sillimanite–quartz are rimmed by cordierite (Fig. 5b). Orthopyroxene–sillimanite–quartz intergrowths also occur as inclusions within the rims of garnet porphyroblasts (Fig. 4d).

Orthopyroxene–sillimanite intergrowths

Fine- to medium-grained intergrowths of orthopyroxene and sillimanite, partially rimming resorbed garnet and cordierite (Fig. 5c), are common in the Type B granulites (e.g. 0101H). In some domains, isolated orthopyroxene–sillimanite intergrowths form pseudomorphs after garnet.

Sapphirine–cordierite symplectites

Symplectites of sapphirine and cordierite with rare plagioclase occur in the Type C granulites, in association with resorbed garnet and orthopyroxene porphyroblasts (Fig. 5d).

Orthopyroxene–cordierite ± spinel symplectites

Fine- to medium-grained orthopyroxene–cordierite symplectites occur as rims around garnet grains (Fig. 5e) in the Type A, B and C granulites. Where garnet is absent (Type D), these symplectites are associated with orthopyroxene porphyroblasts. Where associated with quartz (Type A granulites), orthopyroxene symplectite forms a fine rim on the quartz grains. In Type B granulites the symplectite also contains spinel and Fe–Ti oxides.

Moats and rinds of cordierite

Cordierite in all samples usually forms secondary textures, such as moats, rinds or symplectites. Cordierite with sillimanite forms moats around garnet porphyroblasts in Type A and B granulites (Fig. 5f), and in Type A granulites cordierite forms rims on orthopyroxene–sillimanite–quartz.

Orthopyroxene–sapphirine symplectites

This symplectite is one of the main textural features of the Type C (Fig. 5g) and D (Fig. 5h) granulites. In Type D granulites the symplectite occurs at orthopyroxene porphyroblast grain boundaries, but in Type C granulites it forms rims around strongly resorbed fine-grained garnet and orthopyroxene (Fig. 5g).

Orthopyroxene–spinel symplectites

Some domains in Type C granulites preserve orthopyroxene–spinel symplectite, which rims the sapphirine–orthopyroxene symplectite associated with garnet and orthopyroxene porphyroblasts (Fig. 5i). Rarely, isolated orthopyroxene–spinel symplectite rims orthopyroxene porphyroblasts (Fig. 5j).

Biotite-bearing rims and intergrowths

Biotite is present in all the samples studied, normally as coarse scattered grains or intergrown with cordierite (e.g. Type A granulites) (Fig. 5k). Biotite also forms partial rims around garnet and orthopyroxene porphyroblasts in Type A, B and C granulites (Fig. 5l).

Kornerupine-bearing assemblages

Kornerupine is present only in Type D granulites, where it coexists with cordierite, orthopyroxene porphyroblasts and orthopyroxene–sapphirine symplectite (Fig. 5m).

Orthopyroxene-rims on biotite

In quartz-bearing granulites (Type A), fine-grained orthopyroxene with minor cordierite and K-feldspar form rims on biotite (Fig. 5n).

MINERAL CHEMISTRY

Electron microprobe analyses were carried out using a JEOL JED2140-JSM 5301S-electron microprobe at Okayama University. All analyses were obtained with 'MINM 53' natural mineral samples used as standards. All minerals were analysed for SiO_2, TiO_2, Cr_2O_3, Al_2O_3, FeO, MgO, MnO, CaO, Na_2O and K_2O. Biotite also was analysed for F and Cl, and spinel also for ZnO. The data were reduced by using ZAF correction procedures. Representative analytical data are given in Tables 2, 3, 4 and 5.

Sapphirine

Sapphirine coexisting with quartz as inclusions in garnet porphyroblasts (Type A granulites) has a MAS end-member composition close to 2:2:1 (Fig. 6). Its X_{Mg} [Mg/(Mg + Fe)] value ranges from 0·731 to 0·744. Sapphirine in sapphirine–cordierite symplectites (Types C and D) has an intermediate MAS end-member composition between 2:2:1 and 7:9:3, and X_{Mg} of 0·844–0·847. Sapphirine in sapphirine–orthopyroxene symplectites

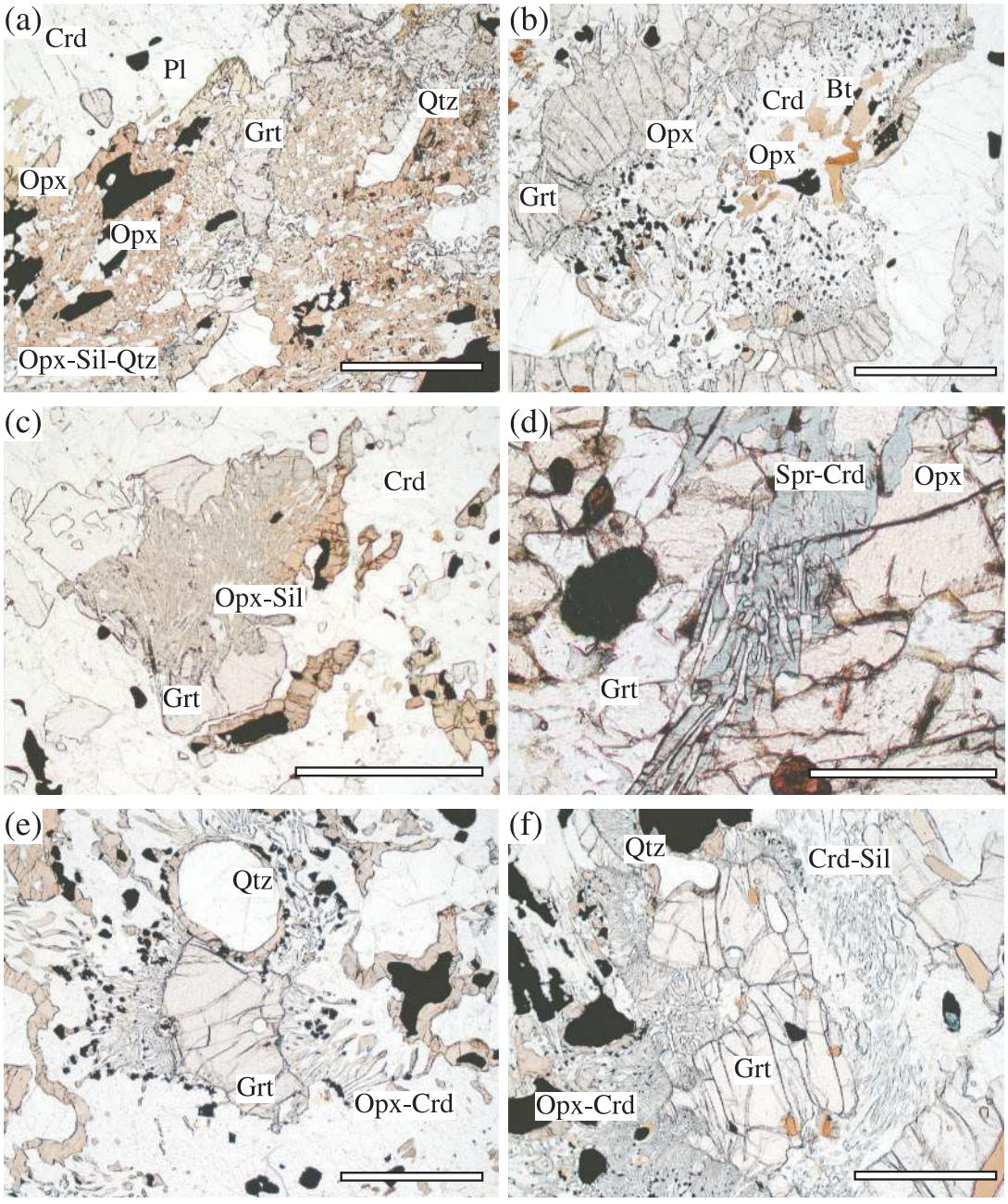

Fig. 5. Photomicrographs of retrograde textures identified from all four rock types. (a) Medium-grained intergrowth of orthopyroxene–sillimanite–quartz in Type A samples. (b) The grain boundary of orthopyroxene–sillimanite–quartz separated by fine rim of cordierite. (c) Orthopyroxene–sillimanite intergrowth after garnet. The matrix represents mainly cordierite with minor K-feldspar and plagioclase. (d) Photomicrograph of sapphirine–cordierite ± plagioclase symplectite formed in the grain boundary of garnet porphyroblast. (e) Orthopyroxene–cordierite symplectite after garnet and quartz. (Note the fine moat of orthopyroxene around quartz grains.) (f) Partial rim of cordierite with sillimanite around garnet. [Note the orthopyroxene–cordierite symplectite on the other side of garnet, with a similar texture to that explained in (e).] (g) Photomicrograph showing relict of fine-grained garnet within orthopyroxene–sapphirine and orthopyroxene–cordierite symplectites. Note the orthopyroxene porphyroblasts on the outer rim of symplectite, a major retrograde texture present in Type C samples.) (h) Similar texture of orthopyroxene–sapphirine ± spinel symplectite observed in Type D samples. (i) Orthopyroxene–spinel symplectite-rim over sapphirine–orthopyroxene symplectite identified only in rare domains of Type C samples. (j) Photomicrograph of isolated orthopyroxene–spinel symplectites in the grain boundary of orthopyroxene porphyroblasts from Type C rock types. (k) Biotite–cordierite symplectite in the rim of garnet porphyroblast. (l) Late biotite-rim on orthopyroxene present in most of the samples. Photomicrograph from Type A samples. (m) Photomicrograph of kornerupine-bearing assemblage in the Type D samples. (n) Late orthopyroxene rim on biotite observed from the matrix of Type A samples. This texture is observed only in quartz-present domains. The scale bars for (d), (i) and (j) represent 0·5 mm, whereas those for (a)–(c), (e)–(h) and (k)–(n) represent 1 mm.

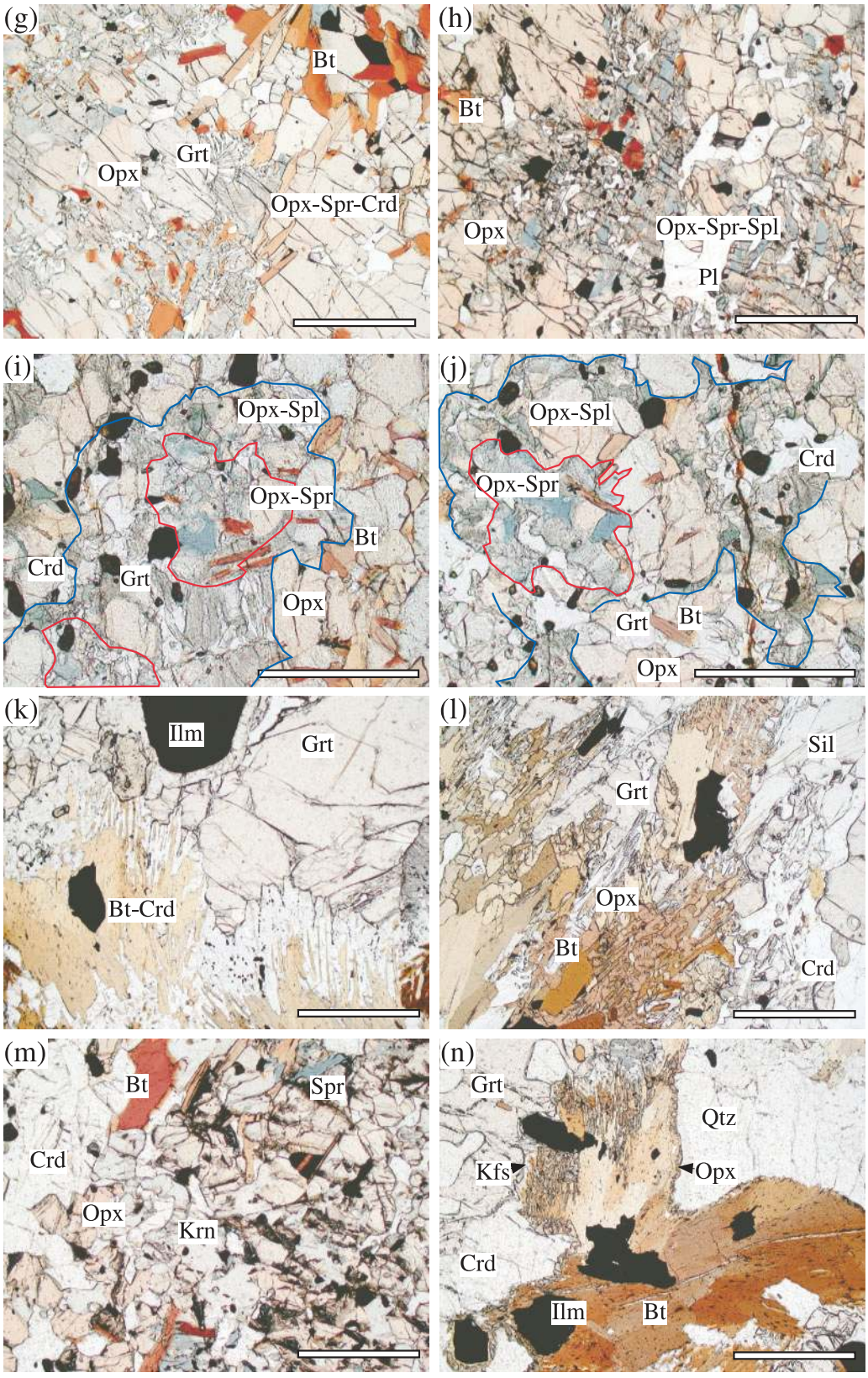

Fig. 5. Continued

Table 2: Representative analyses of sapphirine and garnet

	Sapphirine					Garnet								
Type:	Type A	Type A	Type C	Type C	Type D	Type A	Type A	Type A	Type A	Type B	Type B	Type B	Type C	Type C
Sample no:	3107B	3107B	0505E	0505E	0505A	3107B	3107B	3107B	3107B	0101H	0101H	0101H	0505E	0505E
Texture:	Spr—Qtz	Spr—Qtz	Spr—Opx	Spr—Opx	Spr—Crd	core	core	rim	rim	core	rim	rim	core	rim
SiO_2	16·40	16·70	14·15	14·35	15·40	40·45	40·65	40·45	40·50	40·46	40·40	40·51	40·60	40·58
TiO_2	0·00	0·10	0·00	0·30	0·10	0·00	0·00	0·00	0·00	0·00	0·00	0·00	0·00	0·00
Al_2O_3	56·95	56·80	62·00	61·20	60·50	22·85	22·98	22·86	22·90	22·86	22·83	22·87	22·95	22·94
Cr_2O_3	0·00	0·00	0·30	0·20	0·00	0·00	0·00	0·00	0·00	0·00	0·00	0·00	0·00	0·00
FeO	10·20	10·40	6·20	6·90	5·80	20·72	20·50	21·51	20·82	20·41	21·50	21·50	17·78	21·00
MnO	0·00	0·00	0·00	0·00	0·30	0·70	1·15	0·81	0·60	0·90	0·70	1·20	0·60	0·70
MgO	16·60	16·80	17·40	17·30	18·00	14·60	14·50	14·32	14·30	14·40	13·90	13·70	14·68	14·50
CaO	0·00	0·00	0·00	0·00	0·10	0·60	0·90	0·40	1·10	1·00	0·90	0·90	3·00	0·80
Na_2O	0·00	0·00	0·00	0·00	0·10	0·00	0·00	0·00	0·00	0·00	0·00	0·08	0·00	0·00
K_2O	0·00	0·00	0·00	0·00	0·10	0·10	0·00	0·00	0·10	0·10	0·10	0·00	0·10	0·00
Total	100·15	100·8	100·05	100·25	100·4	100·02	100·68	100·35	100·32	100·13	100·33	100·76	99·71	100·52
Oxygen	10	10	10	10	10	12	12	12	12	12	12	12	12	12
Si	0·983	0·996	0·835	0·848	0·905	3·002	3·000	3·001	3·001	3·001	3·002	3·002	3·002	3·000
Ti	0·000	0·004	0·000	0·013	0·004	0·000	0·000	0·000	0·000	0·000	0·000	0·000	0·000	0·000
Al	4·025	3·992	4·314	4·265	4·192	1·999	1·999	1·999	2·000	1·999	2·000	1·998	2·000	1·999
Cr	0·000	0·000	0·014	0·009	0·000	0·000	0·000	0·000	0·000	0·000	0·000	0·000	0·000	0·000
Fe	0·512	0·519	0·306	0·341	0·285	1·286	1·265	1·334	1·290	1·266	1·336	1·333	1·099	1·298
Mn	0·000	0·000	0·000	0·000	0·015	0·044	0·072	0·051	0·038	0·057	0·044	0·075	0·038	0·044
Mg	1·484	1·493	1·531	1·524	1·577	1·615	1·595	1·583	1·579	1·592	1·539	1·513	1·617	1·597
Ca	0·000	0·000	0·000	0·000	0·006	0·048	0·071	0·032	0·087	0·079	0·072	0·071	0·238	0·063
Na	0·000	0·000	0·000	0·000	0·011	0·000	0·000	0·000	0·000	0·000	0·000	0·011	0·000	0·000
K	0·000	0·000	0·000	0·000	0·007	0·009	0·000	0·000	0·009	0·009	0·009	0·000	0·009	0·000
Total cation	7·004	7·004	7·001	7·001	7·004	8·003	8·001	8·000	8·004	8·004	8·003	8·004	8·003	8·001
Al^{IV}	2·017	2·005	2·165	2·152	2·095	–	–	–	–	–	–	–	–	–
Al^{VI}	2·008	1·987	2·149	2·113	2·097	–	–	–	–	–	–	–	–	–
Fe^{3+}	0·011	0·011	0·002	0·004	0·011	0·010	0·003	0·000	0·012	0·012	0·008	0·013	0·009	0·003
Fe^{2+}	0·500	0·508	0·305	0·338	0·274	1·277	1·262	1·335	1·278	1·254	1·328	1·319	1·090	1·295
X_{Mg}	0·744	0·742	0·833	0·817	0·847	0·557	0·558	0·543	0·550	0·557	0·535	0·532	0·595	0·552
X^*_{Mg}	0·748	0·746	0·834	0·819	0·852	0·559	0·558	0·543	0·553	0·559	0·537	0·534	0·597	0·552
Alm	–	–	–	–	–	0·428	0·421	0·445	0·429	0·421	0·445	0·443	0·365	0·432
Spe	–	–	–	–	–	0·015	0·024	0·017	0·013	0·019	0·015	0·025	0·013	0·015
Pyr	–	–	–	–	–	0·541	0·532	0·528	0·530	0·534	0·516	0·508	0·542	0·533
Grs	–	–	–	–	–	0·012	0·022	0·011	0·024	0·022	0·021	0·019	0·075	0·020
Adr	–	–	–	–	–	0·004	0·001	0·000	0·005	0·005	0·003	0·005	0·004	0·001

Fe^{3+} calculated after charge balance. Texture description: 'in', inclusion and symplectite represented by the involved mineral phases.

Table 3: Selected microprobe analyses of orthopyroxene based on various textural relations

	Orthopyroxene														
Type:	Type A	Type A	Type A	Type B	Type A	Type A	Type A	Type B	Type A	Type C	Type D	Type C	Type C	Type A	Type A
Sample no:	3107B	3107B	3107B	0101H	3107B	3107B	3107B	0101H	3107B	0505E	0505A	0505E	0505E	3107B	3107B
Texture:	in Grt	in Grt	pb core	pb core	pb—rim	Opx—Sil—Qtz	Opx—Sil—Qtz	Opx—Sil	Opx—Crd	Opx—Crd	Opx—Spr	Opx—Spr	Opx—Spl	Opx—rim	Opx—rim
SiO_2	47·10	47·31	47·52	48·10	48·82	49·56	50·15	49·55	50·00	50·45	52·01	51·91	52·10	51·50	51·80
TiO_2	0·50	0·10	0·50	0·20	0·40	0·00	0·00	0·10	0·00	0·30	0·50	0·30	0·00	0·00	0·00
Al_2O_3	12·55	12·82	12·95	11·60	9·82	8·90	8·85	8·80	7·90	8·20	7·25	7·30	7·20	6·50	5·94
Cr_2O_3	0·00	0·10	0·30	0·00	0·10	0·00	0·20	0·10	0·40	0·20	0·20	0·00	0·00	0·00	0·00
FeO	16·60	16·10	15·52	17·50	17·40	17·90	17·20	17·80	18·50	16·60	12·03	12·32	12·11	17·63	17·62
MnO	0·10	0·00	0·10	0·20	0·10	0·00	0·20	0·20	0·40	0·00	0·40	0·10	0·20	0·30	0·10
MgO	21·18	21·79	22·12	21·50	23·00	22·85	23·20	22·60	22·10	23·95	27·82	27·87	27·82	24·42	24·84
CaO	0·70	0·90	0·60	0·10	0·00	0·00	0·00	0·20	0·10	0·00	0·20	0·30	0·10	0·00	0·10
Na_2O	0·20	0·20	0·30	0·30	0·00	0·10	0·30	0·20	0·30	0·30	0·10	0·00	0·10	0·05	0·00
K_2O	0·20	0·00	0·10	0·10	0·10	0·10	0·00	0·00	0·00	0·00	0·00	0·00	0·00	0·00	0·00
Total	99·13	99·32	100·01	99·60	99·74	99·41	100·10	99·55	99·70	100·00	100·51	100·10	99·63	100·40	100·40
Oxygen	6	6	6	6	6	6	6	6	6	6	6	6	6	6	6
Si	1·726	1·724	1·717	1·756	1·779	1·813	1·817	1·812	1·834	1·824	1·836	1·838	1·851	1·862	1·872
Ti	0·014	0·003	0·014	0·005	0·011	0·000	0·000	0·003	0·000	0·008	0·013	0·008	0·000	0·000	0·000
Al	0·542	0·551	0·551	0·499	0·422	0·384	0·378	0·379	0·342	0·349	0·302	0·305	0·301	0·277	0·253
Cr	0·000	0·003	0·009	0·000	0·003	0·000	0·006	0·003	0·012	0·006	0·006	0·000	0·000	0·000	0·000
Fe	0·509	0·491	0·469	0·534	0·530	0·548	0·521	0·544	0·567	0·502	0·355	0·365	0·360	0·533	0·532
Mn	0·003	0·000	0·003	0·006	0·003	0·000	0·006	0·006	0·012	0·000	0·012	0·003	0·006	0·009	0·003
Mg	1·157	1·183	1·191	1·170	1·249	1·246	1·253	1·232	1·208	1·290	1·463	1·471	1·473	1·316	1·338
Ca	0·027	0·035	0·023	0·004	0·000	0·000	0·000	0·008	0·004	0·000	0·008	0·011	0·004	0·000	0·004
Na	0·014	0·014	0·021	0·021	0·000	0·007	0·021	0·014	0·021	0·021	0·007	0·000	0·007	0·004	0·000
K	0·009	0·000	0·005	0·005	0·005	0·005	0·000	0·000	0·000	0·000	0·000	0·000	0·000	0·000	0·000
Total cation	4·001	4·004	4·002	4·001	4·001	4·001	4·002	4·001	4·000	4·001	4·001	4·001	4·002	4·001	4·002
Al^{IV}	0·275	0·278	0·284	0·244	0·222	0·188	0·184	0·189	0·166	0·176	0·165	0·162	0·150	0·138	0·129
Al^{VI}	0·267	0·273	0·267	0·255	0·200	0·196	0·194	0·191	0·175	0·173	0·137	0·142	0·151	0·139	0·124
X_{Al}	0·271	0·275	0·276	0·250	0·211	0·192	0·189	0·190	0·171	0·175	0·151	0·152	0·151	0·139	0·126
Fe^{3+}	0·003	0·011	0·007	0·004	0·002	0·004	0·005	0·004	0·001	0·002	0·003	0·004	0·005	0·003	0·005
Fe^{2+}	0·505	0·480	0·462	0·530	0·528	0·544	0·516	0·541	0·567	0·500	0·352	0·361	0·354	0·530	0·527
X_{Mg}	0·695	0·707	0·717	0·686	0·702	0·695	0·706	0·693	0·680	0·720	0·805	0·801	0·804	0·712	0·715
X^*_{Mg}	0·696	0·711	0·721	0·688	0·703	0·696	0·708	0·695	0·681	0·721	0·806	0·803	0·806	0·713	0·717

Fe^{3+} calculated after charge balance. Texture description: 'in', inclusion; 'pb', porphyroblast and symplectite represented by the involved mineral phases.

Table 4: Selected analyses for spinel and cordierite according to various textural relations

	Spinel				Cordierite				
Type:	Type A	Type B	Type C	Type C	Type A	Type B	Type C	Type A	Type A
Sample no:	3107B	0101H	0505E	0505E	3107B	0101H	0505E	3107B	3107B
Texture:	in matrix	in matrix	Opx–Spl	Opx–Spl	pb	moat	Spr–Crd	Opx–Crd	with Opx
SiO_2	0·00	0·00	0·00	0·00	50·33	50·14	50·23	49·78	50·05
TiO_2	0·00	0·05	0·05	0·00	0·00	0·00	0·00	0·00	0·00
Al_2O_3	63·95	64·70	65·00	65·10	34·22	34·08	34·15	33·80	34·00
Cr_2O_3	0·50	0·30	0·10	0·10	0·00	0·00	0·00	0·00	0·00
FeO	21·00	19·30	18·62	19·67	2·69	2·90	2·30	2·30	1·80
MnO	0·00	0·00	0·00	0·00	0·10	0·00	0·00	0·00	0·00
MgO	13·73	15·01	15·60	14·90	11·80	11·67	12·20	12·00	12·40
CaO	0·00	0·20	0·10	0·00	0·00	0·10	0·00	0·00	0·00
Na_2O	0·00	0·00	0·00	0·00	0·00	0·00	0·00	0·05	0·00
K_2O	0·00	0·00	0·10	0·00	0·20	0·10	0·00	0·00	0·00
ZnO	0·00	0·00	0·00	0·00	0·00	0·00	0·00	0·00	0·00
Total	99·18	99·56	99·57	99·77	99·34	98·99	98·88	97·93	98·25
Oxygen	4	4	4	4	18	18	18	18	18
Si	0·000	0·000	0·000	0·000	4·999	4·999	4·997	5·001	4·999
Ti	0·000	0·001	0·001	0·000	0·000	0·000	0·000	0·000	0·000
Al	1·988	1·987	1·989	1·995	4·007	4·005	4·004	4·002	4·003
Cr	0·010	0·006	0·002	0·002	0·000	0·000	0·000	0·000	0·000
Fe	0·463	0·420	0·404	0·428	0·223	0·242	0·191	0·193	0·150
Mn	0·000	0·000	0·000	0·000	0·008	0·000	0·000	0·000	0·000
Mg	0·540	0·583	0·603	0·577	1·747	1·734	1·809	1·797	1·846
Ca	0·000	0·006	0·003	0·000	0·000	0·011	0·000	0·000	0·000
Na	0·000	0·000	0·000	0·000	0·000	0·000	0·000	0·010	0·000
K	0·000	0·000	0·003	0·000	0·025	0·013	0·000	0·000	0·000
Zn	0·000	0·000	0·000	0·000	0·000	0·000	0·000	0·000	0·000
Total cation	3·001	3·003	3·005	3·002	11·010	11·004	11·001	11·003	10·999
Fe^{3+}	0·002	0·007	0·014	0·004	0·000	0·000	0·000	0·000	0·000
Fe^{2+}	0·461	0·414	0·390	0·423	0·223	0·242	0·191	0·193	0·150
X_{Mg}	0·538	0·581	0·599	0·574	0·887	0·878	0·904	0·903	0·925
X^*_{Mg}	0·539	0·585	0·607	0·577	0·887	0·878	0·904	0·903	0·925

Fe^{3+} calculated after charge balance. Texture description: 'pb', porphyroblast and symplectite represented by the involved mineral phases.

(Types C and D) has a composition near 7:9:3 with X_{Mg} of 0·817–0·833 (Fig. 6). These compositional variations are comparable with those reported for sapphirine from adjacent UHT terranes (e.g. Harley *et al.*, 1990). There is only a slight difference between X_{Mg} and X^*_{Mg} (Mg/Mg + Fe^{2+}) values owing to the sapphirine's low Fe^{3+} content.

Garnet

In all garnet-bearing samples, porphyroblasts or relicts within the symplectites preserve pyrope–almandine solid solutions with less than 7·5–1·1 mol % grossular and 2·4–1·3 mol % spessartine. Garnet cores with inclusions of sapphirine–quartz (3107B) preserve the highest Mg content (Prp up to 54·1 mol %). The garnet rims with inclusions of orthopyroxene, quartz and sillimanite have a slightly lower Mg content (Prp 53·2 mol %). The range of garnet core compositions is $Prp_{54·1–53·2}$, $Alm_{42·8–42·1}$, $Sps_{2·4–1·5}$, $Grs_{2·2–1·2}$ (in mol %). In contrast, the rims associated with orthopyroxene porphyroblasts (3107B, 0101H), multiphase symplectites (3107B, 0505E) or moats and rinds of cordierite (3107B) are relatively almandine rich ($Prp_{53·3–48·2}$, $Alm_{44·5–49·8}$, $Sps_{2·5–1·3}$,

Table 5: Representative microprobe analyses for biotite and kornerupine

	Biotite					Kornerupine			
Type:	Type A	Type B	Type A	Type C	Type A	Type C	Type C	Type C	Type C
Sample no:	3107B	0101H	3107B	0505E	3107B	0505E	0505E	0505E	0505E
Texture:	in matrix	in Grt	Bt–Crd	Bt–Crd	Bt rim	in matrix	in matrix	in matrix	in matrix
SiO_2	38·60	38·70	38·40	40·10	39·20	30·20	31·00	30·21	31·10
TiO_2	4·40	4·10	4·30	3·40	3·50	0·30	0·20	0·70	0·40
Al_2O_3	16·10	16·80	15·80	15·80	16·80	43·90	43·00	44·40	43·30
Cr_2O_3	0·00	0·10	0·20	0·00	0·00	0·10	0·00	0·10	0·00
FeO	10·00	9·10	9·70	9·20	7·60	5·60	4·50	4·70	4·90
MnO	0·00	0·00	0·30	0·00	0·00	0·20	0·50	0·00	0·00
MgO	16·80	17·00	17·30	18·20	18·60	17·00	16·80	16·40	17·20
CaO	0·00	0·00	0·00	0·00	0·00	0·10	0·30	0·00	0·20
Na_2O	0·00	0·30	0·20	0·00	0·00	0·10	0·10	0·00	0·10
K_2O	10·20	10·10	10·20	9·60	10·00	0·00	0·00	0·00	0·00
F	0·17	0·02	0·22	0·00	0·00	–	–	–	–
Cl	0·09	0·03	0·05	0·00	0·00	–	–	–	–
F=O	0·07	0·01	0·09	0·00	0·00	0·00	0·00	0·00	0·00
Cl=O	0·02	0·01	0·01	0·00	0·00	0·00	0·00	0·00	0·00
H_2O^*	4·05	4·16	4·03	4·20	4·19	1·21	1·20	1·20	1·21
Total	100·31	100·39	100·60	100·50	99·89	98·71	97·60	97·71	98·41
Oxygen	22	22	22	22	22	21	21	21	21
Si	5·580	5·562	5·547	5·721	5·606	3·753	3·876	3·766	3·855
Ti	0·478	0·443	0·467	0·365	0·376	0·028	0·019	0·066	0·037
Al	2·743	2·846	2·690	2·657	2·832	6·430	6·336	6·523	6·326
Cr	0·000	0·011	0·023	0·000	0·000	0·010	0·000	0·010	0·000
Fe	1·209	1·094	1·172	1·098	0·909	0·582	0·470	0·490	0·508
Mn	0·000	0·000	0·037	0·000	0·000	0·021	0·053	0·000	0·000
Mg	3·620	3·643	3·726	3·871	3·966	3·150	3·131	3·048	3·179
Ca	0·000	0·000	0·000	0·000	0·000	0·013	0·040	0·000	0·027
Na	0·000	0·084	0·056	0·000	0·000	0·024	0·024	0·000	0·024
K	1·881	1·852	1·880	1·747	1·824	0·000	0·000	0·000	0·000
Total cation	15·511	15·534	15·597	15·459	15·514	14·011	13·950	13·902	13·956
F	0·078	0·009	0·100	0·000	0·000	–	–	–	–
Cl	0·022	0·007	0·012	0·000	0·000	–	–	–	–
OH^*	3·900	3·984	3·887	4·000	4·000	0·156	0·131	0·138	0·138
X_{Mg}	0·750	0·769	0·761	0·779	0·814	0·844	0·869	0·862	0·862

H_2O^* and OH^* content calculated according to stoichiometry.

$Grs_{2·1–1·1}$ mol %). Droop & Bucher-Nurminen (1984) reported similar compositional features in garnet from the sapphirine-bearing granulites of the Gruf Complex, Italian Central Alps.

Orthopyroxene

The composition of orthopyroxene differs with textural setting (Fig. 7). Orthopyroxene cores in porphyroblasts and inclusions in garnet (Type A granulites) preserve the highest Al contents (up to Al_2O_3 12·95 wt %), with X_{Mg} ranging from 0·717 to 0·695. Fine-grained orthopyroxene in the matrix, and the rims of orthopyroxene porphyroblasts, are low in Al and Mg (Al_2O_3 9·82–9·80 wt %; X_{Mg} 0·686–0·679). Orthopyroxene in orthopyroxene–sillimanite–quartz intergrowths (Type A) (Al_2O_3 8·90–8·79 wt %; X_{Mg} 0·708–0·692) and in orthopyroxene–sillimanite intergrowths (Type B) (Al_2O_3 8·80–7·61 wt %;

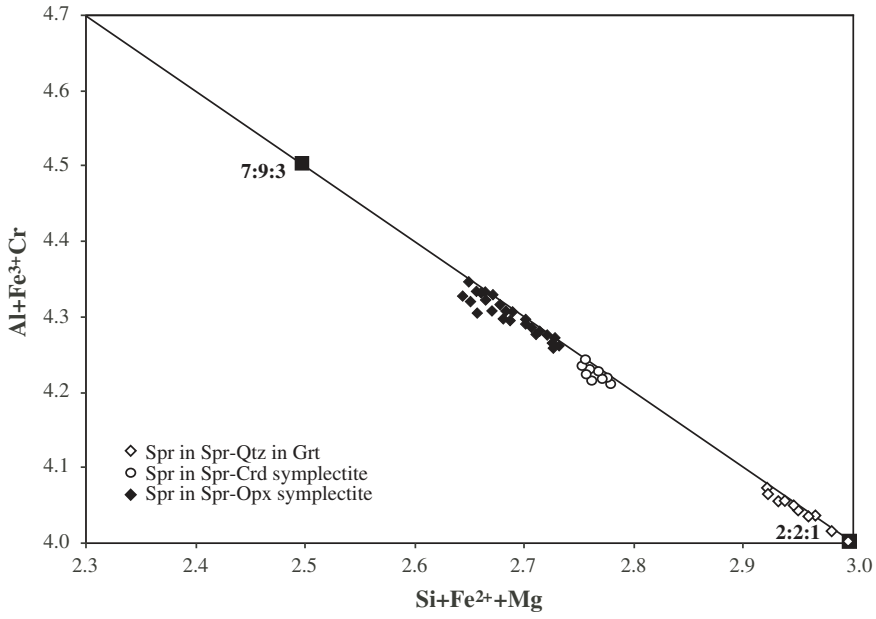

Fig. 6. Composition of sapphirine plotted on (Si+Fe^{2+}+Mg) vs (Al+Fe^{3+}+ Cr) diagram. Near-peak sapphirine (inclusion in garnet) preserves a composition near 2:2:1. The sapphirines involved in retrograde symplectites have a composition between 7:9:3 and 2:2:1.

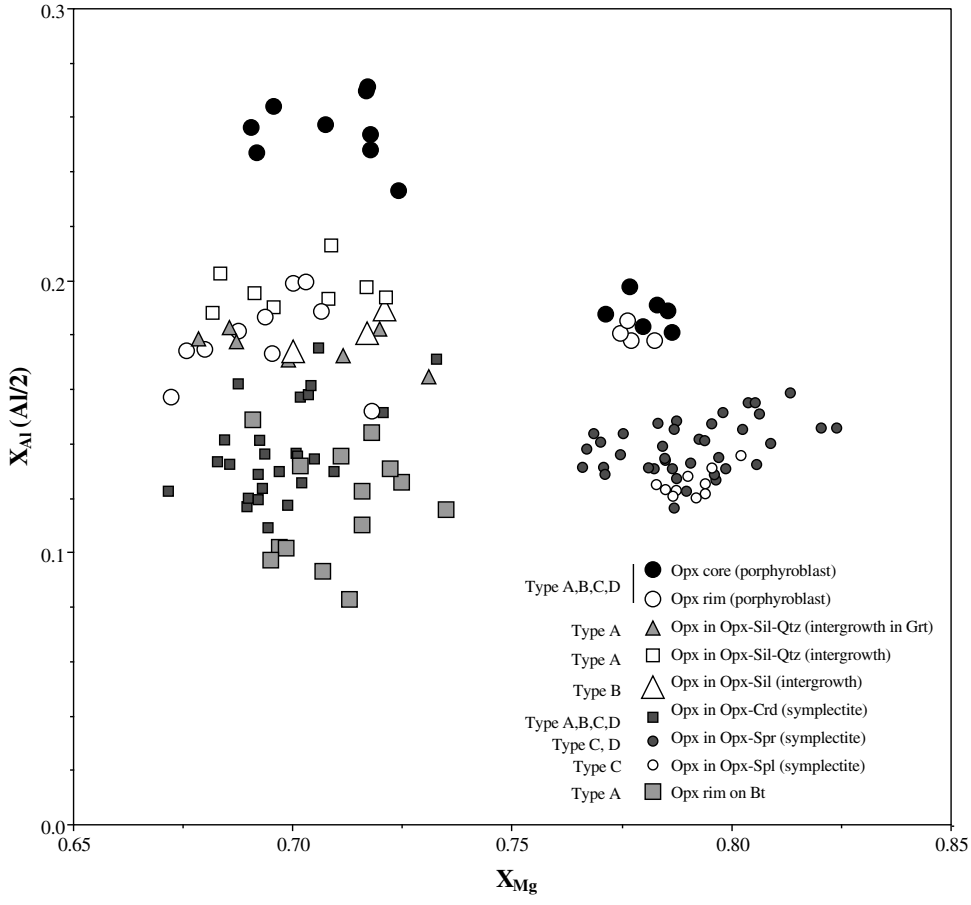

Fig. 7. X_{Al} vs X_{Mg} plot of orthopyroxene compositions with respect to each textural feature.

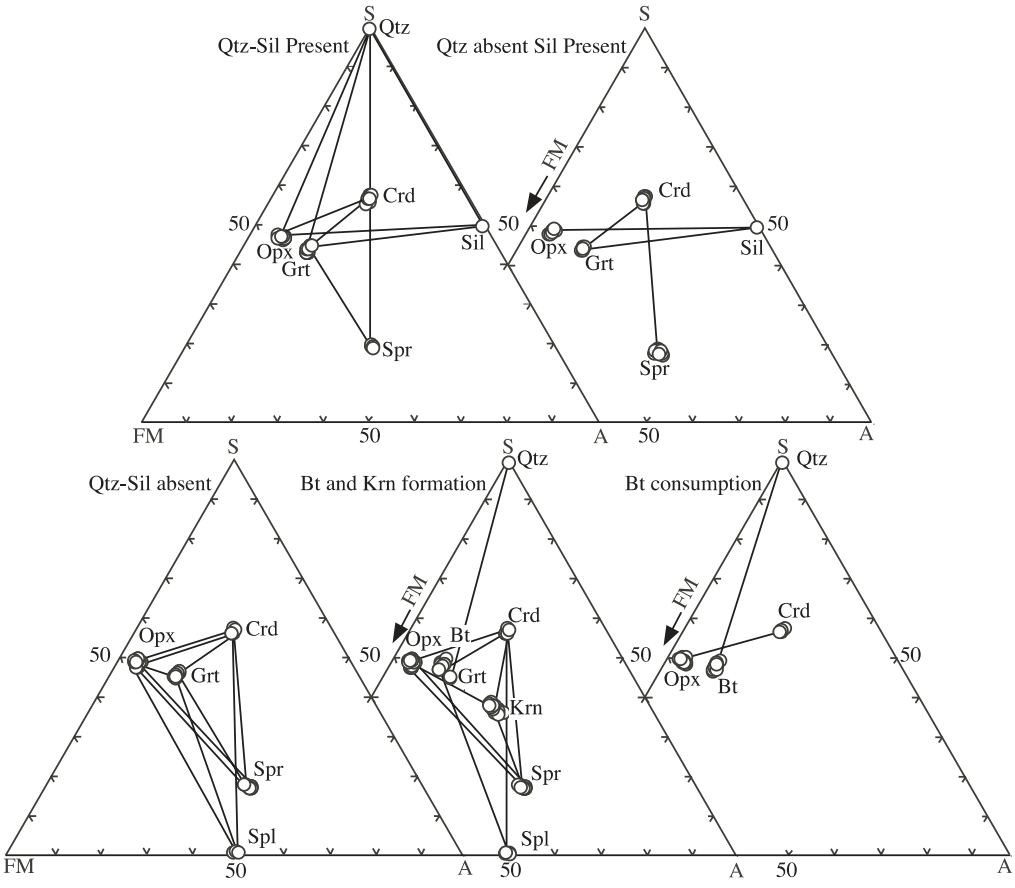

Fig. 8. SiO_2–(FeO + MgO)–Al_2O_3 plots for all major mineral composition for Type A, B, C and D samples, separately. The tie-lines represent mineral reactions explained in the text.

X_{Mg} 0·708–0·695) preserves similar compositions, although the latter is slightly lower in Al. Orthopyroxene in orthopyroxene–cordierite symplectites (e.g. Types B and C) (Al_2O_3 8·20–7·93 wt %; X_{Mg} 0·720–0.680) and orthopyroxene–sapphirine symplectites (Types C and D) (Al_2O_3 7·30–6·91 wt %; X_{Mg} 0·805–0·792) preserves similar compositions, although, in the latter, Al is slightly lower and Mg higher. The orthopyroxene–spinel symplectites have slightly lower Al_2O_3 (7·20–6·71 wt %), with X_{Mg} ranging from 0·809 to 0·805. Orthopyroxene in orthopyroxene-rims on biotite (Type A) has the lowest Al content but is slightly enriched in Mg (Al_2O_3 6·50–5·75 wt %; X_{Mg} 0·726–0·713). A minor amount of Fe^{3+} in all the orthopyroxene slightly enhances the X_{Mg} values. Similar compositions have been observed in other UHT terranes (e.g. Harley *et al.*, 1990).

Cordierite

Cordierite occurs mainly in retrograde textures. The cordierite porphyroblasts give an oxide total of >99·34 wt %, but the totals for cordierite in moats and symplectites is lower, at >97·95 wt %, indicating minor volatiles in the crystal structure. No attempt has been made to estimate the composition of the volatiles, nor are there any ion microprobe data on the CO_2 or H_2O contents of cordierite from UHT granulites elsewhere in the Highland Complex. Kriegsman & Schumacher (1999) suggested, on the basis of birefringence, that the cordierite in the UHT granulites contains more H_2O than CO_2. The samples discussed here are similar. Cordierite inclusions in garnet-rims (Type A) have the lowest X_{Mg} (0·889), whereas cordierite in symplectites and moat textures has slightly higher X_{Mg} values (0·925–0·878).

Spinel

Spinel is relatively rare in all the studied samples. It occurs in some quartz-absent granulites (Type B) in symplectites or as lobate grains in the matrix. Spinel in orthopyroxene–spinel symplectites (Type C) has an X_{Mg} range of 0·607–0·569, and lobate spinel associated with kornerupine, cordierite and orthopyroxene (Type D) in quartz-, sillimanite- and garnet-absent domains preserves

X_{Mg} values of 0·585–0·529. The spinel Zn and Cr contents are low. The X^{*}_{Mg} values are slightly elevated by the presence of minor Fe^{3+}.

Biotite

The composition of biotite is very similar in all textural settings. F is uniformly low (e.g. Types A, B and C), but TiO_2 ranges from 4·4 to 3·2 wt %. Biotite rims in contact with mafic phases (e.g. Type A) preserve a Ti content of 0·376–0·331 p.f.u. and an X_{Mg} range of 0·819–0·799. Biotite inclusions in Type A, B and C granulites preserve an X_{Mg} of 0·769–0·756, with 0·468–0·431 p.f.u. of Ti, but biotite in symplectitic association with cordierite (e.g. Type B) preserves 0·371–0·360 p.f.u. of Ti and an X_{Mg} of 0·801–0·776.

Kornerupine

The low oxide total (<98·71 wt %) of kornerupine in Type D granulites indicates the presence of H_2O and boron in the crystal structure. The X_{Mg} in kornerupine ranges from 0·869 to 0·842.

Feldspars

Feldspars include K-feldspar, plagioclase, perthites and minor antiperthites. K-feldspar preserves a composition of $Or_{84·0–82·6}Ab_{18·4–16·0}An_{0·0}$. Plagioclase cores retain the peak composition ($An_{29·0–28·6}$), whereas the rims ($An_{36·0–32·9}$) are mainly in contact with garnet and orthopyroxene (e.g. Type A).

Fe–Ti oxides

Opaque phases are mainly ilmenite with fine lamellae of exsolved magnetite. The ilmenite is almost pure $FeTiO_3$, whereas the magnetite contains minor Ti. The opaque inclusions in garnet, sapphirine and orthopyroxene are mostly rutile and minor ilmenite. Ilmenite in the matrix and inclusions preserves similar compositions. Rutile is almost pure, with 99 wt % of TiO_2.

MINERAL REACTIONS

The reaction textures discussed above can be explained by using the K_2O–FeO–MgO–Al_2O_3–SiO_2–H_2O (KFMASH) and FeO–MgO–Al_2O_3–SiO_2 (FMAS) systems. Most near-peak assemblages, such as garnet–sapphirine–quartz–K-feldspar or orthopyroxene–sillimanite–quartz–K-feldspar, are strongly overprinted by late orthopyroxene–sapphirine–cordierite, biotite–cordierite–kornerupine or orthopyroxene–cordierite–K-feldspar assemblages. The compositions of minerals in each textural setting and assemblage are shown in SiO_2–Al_2O_3–[FeO+MgO] (S–A–FM) diagrams in Fig. 8. The tie-lines represent the reactions between mineral phases, as described below. Mineral abbreviations follow Kretz (1983).

FMAS system reactions in Type A assemblages

The coexistence of sapphirine–quartz only as inclusions in garnet porphyroblasts (Fig. 4a, b and c) in Type A granulites can be explained by the following reactions:

$$\mathrm{Spr} + \mathrm{Qtz} = \mathrm{Grt} + \mathrm{Sil} \quad (1a)$$

$$\mathrm{Grt} + \mathrm{Spr} + \mathrm{Qtz} = \mathrm{Opx} + \mathrm{Sil}. \quad (1b)$$

Thin rims and moats of cordierite at the boundaries between orthopyroxene, sillimanite and quartz in some domains (3107B) (Fig 5b) reflect the well-documented FMAS continuous reaction

$$\mathrm{Opx} + \mathrm{Sil} + \mathrm{Qtz} = \mathrm{Crd}. \quad (2a)$$

Minor inclusions of orthopyroxene–sillimanite intergrowth with rare quartz inclusions in garnet rims and cordierite with sillimanite inclusions present in Type A granulites (3107B) are evidence for the FMAS univariant reaction

$$\mathrm{Opx} + \mathrm{Sil} + \mathrm{Qtz} = \mathrm{Grt} + \mathrm{Crd}. \quad (2b)$$

Similar reactions have been reported by Droop (1989).

The Fe–Mg zoning profiles of garnets associated with, or partly rimmed by, low-Al and Fe-rich orthopyroxene-forming symplectites with cordierite show an increase in Fe towards the rim. The symplectites also contain minor plagioclase (3107B). The formation of orthopyroxene and cordierite (± plagioclase) after garnet (Fig. 5e) can be explained by the following reaction:

$$\mathrm{Grt} + \mathrm{Qtz} = \mathrm{Opx} + \mathrm{Crd} \pm \mathrm{Pl}. \quad (3)$$

Reactions in Type B assemblages

The orthopyroxene–sillimanite intergrowth (Fig. 5c) on the grain boundary of garnet and cordierite in Type B granulites (0101H) can be explained by the FMAS continuous reaction

$$\mathrm{Grt} + \mathrm{Crd} = \mathrm{Opx} + \mathrm{Sil}. \quad (4)$$

The FMAS continuous reaction, which consumed sillimanite in the presence of orthopyroxene or garnet to produce sapphirine–cordierite symplectite (0505E,

0505A) (Fig. 5d), resulted from the following reactions:

$$\text{Opx} + \text{Sil} = \text{Spr} + \text{Crd} \quad (5a)$$

$$\text{Grt} + \text{Sil} = \text{Spr} + \text{Crd}. \quad (5b)$$

It is noteworthy that these textures are present in Type C and D granulites, in which sillimanite is now absent. In some sillimanite-absent domains, sapphirine–cordierite formation is assumed to have consumed all sillimanite. Later modification of sapphirine–cordierite symplectites to sapphirine–cordierite–plagioclase symplectites is also observed in some domains. Harley *et al.* (1990) reported similar textural phenomena from the orthopyroxene–sillimanite granulites of Forefinger Point, East Antarctica.

Reactions in Type C assemblages

Garnet porphyroblasts associated with orthopyroxene–cordierite and sapphirine–orthopyroxene symplectites (0505E) represent the main symplectite-forming reaction (Fig. 5g), which produced the 'inter-fingering' textures surrounding garnet. Garnet breakdown in the absence of quartz and sillimanite produced orthopyroxene–cordierite symplectites, and sapphirine–orthopyroxene symplectite or orthopyroxene–sapphirine–cordierite symplectite at its grain boundary (Fig. 5g). This can be explained by the reaction

$$\text{Grt} = \text{Opx} + \text{Spr} + \text{Crd}. \quad (6)$$

The high-Al orthopyroxene–sapphirine symplectites partly rimmed by fine-grained low-Al orthopyroxene–spinel symplectite in garnet-bearing and quartz- and sillimanite-absent rock types (0505E) (Fig. 5i and j) could be produced by the reaction

$$\text{High-Al Opx} + \text{Spr} = \text{Low-Al Opx} + \text{Spl (symplectite)}. \quad (7)$$

Biotite-forming reactions

One reactant in the biotite-forming reactions must have contained K. These reactions involved the consumption of pre-existing K-feldspar or the early consumption of other phases such as vapour (V) or melt (L). There is no definitive field or textural evidence for the former presence of melt. The presence of a vapour phase is therefore most likely, even though some textures might have involved melt.

The intergrowth of biotite with cordierite (3107B) at the rim of garnet porphyroblasts with minor associated K-feldspar extends the reaction towards the KFMASH by decreasing the amount of K-feldspar (Fig. 5k), which can be explained by the retrograde hydration reaction

$$\text{Grt} + \text{Kfs} + \text{Qtz} + \text{V} = \text{Bt} + \text{Crd}. \quad (8)$$

Similar reactions involving melt, such as

$$\text{Opx} + \text{Kfs} + \text{L} = \text{Bt} + \text{Crd} \quad (9)$$

in the absence of garnet, is rarely observed. In some domains, owing to the extensive formation of biotite rims on other phases (Fig. 5l), K-feldspar was completely consumed and the amount of cordierite increased. Additional formation of biotite at the expense of orthopyroxene–sapphirine symplectites [which are associated with biotite–cordierite intergrowths (0505A) and minor plagioclase], can be explained through the reaction

$$\text{Opx} + \text{Spr} + \text{Kfs} + \text{V} = \text{Bt} + \text{Crd} + \text{Pl}. \quad (10)$$

Further modification of the assemblage took place through the univariant reaction that resulted in the production of spinel plus cordierite and biotite:

$$\text{Opx} + \text{Spr} + \text{V} = \text{Bt} + \text{Crd} + \text{Spl}. \quad (11)$$

Kornerupine-forming reactions in Type D assemblages

The formation of kornerupine in quartz-, sillimanite- and garnet-absent samples (0505A) resulted from a reaction that involved sapphirine, orthopyroxene and cordierite (Fig. 5m):

$$\text{Spr} + \text{Opx} + \text{Crd} + \text{V} = \text{Krn}. \quad (12)$$

Kornerupine occurs only locally in the central Highland Complex. The lack of other boron-bearing minerals in the surrounding area and the lack of ion-microprobe data for our kornerupine samples leave the presence and occurrence of boron uncertain. It was probably derived from vapour or associated melt.

Orthopyroxene-rims after biotite consumption

The localized reaction texture in quartz-bearing samples (3107B) whereby low-Al orthopyroxene–cordierite and minor K-feldspar form a rim on biotite in the presence of plagioclase (Fig. 5n) can be explained by the divariant reaction

$$\text{Bt} + \text{Qtz} \pm \text{Pl} = \text{Opx} + \text{Kfs} + \text{Crd} + \text{V}. \quad (13)$$

TEXTURAL INTERPRETATION AND *P–T* HISTORY

The assemblages and reaction textures in the samples studied here are best explained using the KFMASH system. The high-temperature assemblages and reactions

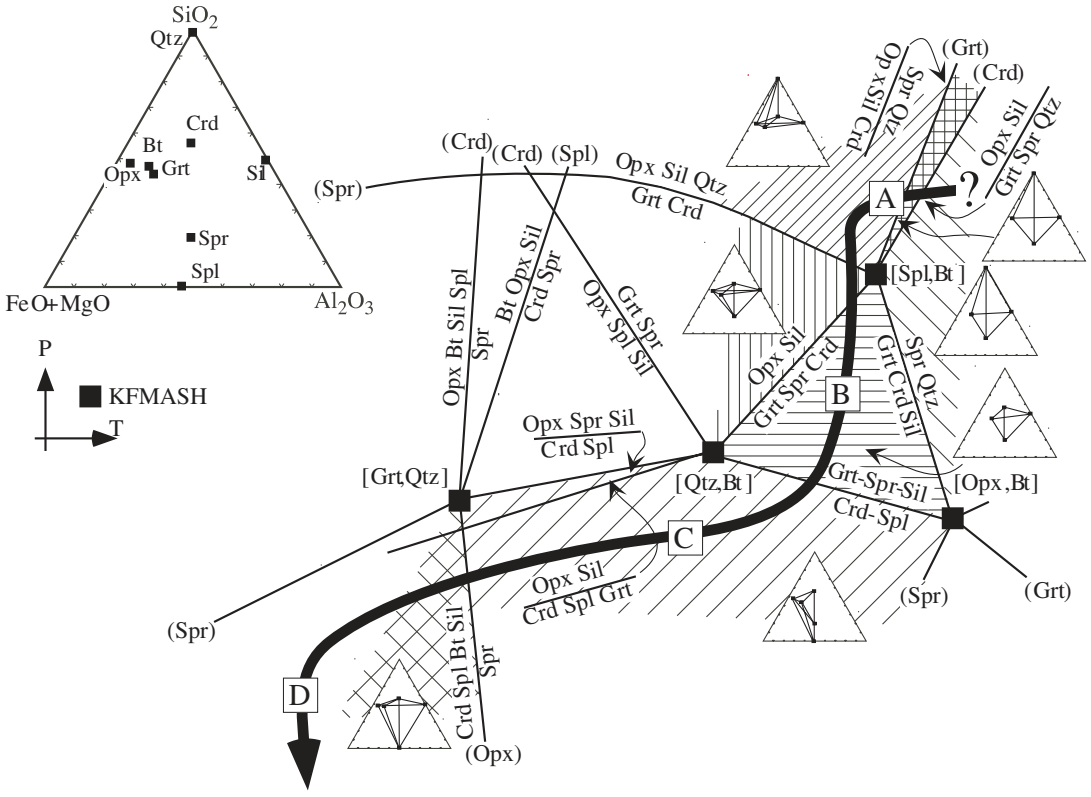

Fig. 9. Modified version of KFMASH grid considering melt and K-feldspar in excess (after McDade & Harley, 2001) (see text for explanation). A, B, C and D represent each segment of evolution.

can be explained by using FMAS reactions, and the K- and H_2O-bearing assemblages are retrograde products. In applying the KFMASH petrogenetic grid, we have taken into account the results of Hensen (1971, 1986), Hensen & Green (1973), Hensen & Harley (1990), Carrington & Harley (1995) and McDade & Harley (2001). The partial pressure of oxygen (fO_2) is a major factor controlling the stability and metastability of invariant points (Hensen, 1986). The mineral reactions and presence of ilmenite inclusions in garnet and orthopyroxene in the Highland Complex granulites are consistent with fO_2 remaining low throughout their evolution.

In the KFMASH system, at low fO_2, the spinel- and biotite-absent invariant point (hereafter [Spl,Bt] for absent phases at invariant points) is fixed at *c.* 11 kbar and just below 1050°C. The position of this point is determined from the FMAS experiments of Hensen (1971) and Hensen & Green (1973). The [Opx,Qtz] invariant is fixed at 8·5–9 kbar and above 1050°C (Hensen & Green, 1973; Hensen, 1987). The [Qtz,Bt] invariant point is fixed at 8–9 kbar, 950°C, although its position is highly sensitive to the Ca and Mn contents of the garnet. The stability of the [Spl,Bt], [Qtz,Bt] and [Grt,Qtz] invariant points is closely related to the evolution of a quartz-poor assemblage. Recent studies of the KFMASH system by McDade & Harley (2001), using the experimental results of Carrington & Harley (1995), supported the revised topology for the petrogenetic grid suggested by Hensen & Harley (1990). Carrington & Harley (1995) fixed the [Spr,Spl] invariant point at 900°C and 8·8 kbar, which is slightly lower than, or similar to, the [Grt,Qtz] invariant point. The new petrogenetic grid of McDade & Harley (2001), projected from melt and K-feldspar, considered the [Crd,Qtz], [Spr,Qtz], [Bt,Qtz] and [Grt,Qtz] invariant points to be metastable. Their proposed grid is therefore, in effect, the inverse projection of that of Hensen & Harley (1990). Here, we use a redrawn version of the Hensen & Harley (1990) grid after McDade & Harley (2001) (Fig. 9).

The textural relationship of kornerupine with sapphirine, orthopyroxene, cordierite and spinel in garnet- and quartz-free domains indicates that it was formed during the retrograde stage of evolution. The stability field of kornerupine should, therefore, fall on the low pressure–temperature side of the [Grt,Qtz] invariant point in the KFMASH system. Seifert (1975) explained kornerupine stability using the MASH system and suggested univariant reactions for kornerupine formation, similar to those described above. The invariant points of [Chl,Spl,Crn] and [Chl,Crd,Crn] referred to by Seifert (1975) and

Goscombe (1992) correspond to KFMASH invariant points [Grt,Qtz] and [Crd,Qtz], respectively. Droop (1989) proposed the stability field for kornerupine-bearing assemblages by using a FMASH grid. On that grid, the assemblage we observe corresponds to reactions on the low pressure–temperature side of the [Ged] invariant point. Goscombe (1992) suggested that kornerupine is stable at 750–950°C and *c.* 5 kbar. We conclude, therefore, that kornerupine from the Highland Complex was formed on the low *P–T* side of the [Grt,Qtz] invariant point. This is consistent with the evolution of kornerupine-absent assemblages and also indicates that kornerupine-bearing and -absent assemblages may follow the same *P–T* path.

The KFMASH petrogenetic grid makes it possible to trace two stages of isobaric cooling and two stages of isothermal decompression. Initial isobaric cooling occurred above the [Spl,Bt] invariant point and can be explained by reactions (1a) and (1b). FMAS continuous reactions (2a) and (2b) represent initial near-isothermal decompression on the low-temperature side of the [Spl,Bt] invariant. Following orthopyroxene–sillimanite intergrowth [reaction (4)], sapphirine–cordierite symplectites [reactions (5a) and (5b)] and orthopyroxene–cordierite ± plagioclase symplectite [reaction (3)] formed through continuous reaction during decompression. A near-isobaric cooling profile is indicated by the formation of orthopyroxene–sapphirine symplectite through reaction (6). Later, low-Al orthopyroxene–spinel symplectite formed by reaction (7) during further cooling.

More complex biotite- or kornerupine-bearing KFMASH reactions occurred during cooling. KFMASH reactions were initiated below the [Qtz,Bt] and [Grt,Qtz] invariant points through reaction (8), and the assemblage was modified further below the [Grt,Qtz], invariant point with the formation of biotite [reactions (9)–(11)]. At that stage, kornerupine also formed [reaction (12)] in the few granulites with quartz-, sillimanite- and garnet-absent domains (Type D). The final stage of near-isothermal decompression involved the breakdown of biotite to form orthopyroxene and cordierite by KFMASH [reaction (13)]. Harley *et al.* (1990) have pointed out that this reaction takes place below 800°C by comparison with the *P–T–X* grid of Hensen & Harley (1990) for their high-a_{SiO_2} samples from Forefinger Point, East Antarctica. Martignole & Martelat (2003) have also described a similar reaction resulting from decompression at *c.* 900°C. Based on all these observations, we conclude that the peak metamorphic *P–T* must have exceeded 11 kbar and 1050°C, i.e. been towards the high *P–T* side of the [Spl,Bt] invariant point where sapphirine–quartz is stable. The FMAS continuous reactions during the isothermal decompression must have occurred below 1050°C, namely on the lower-temperature side of the [Spl,Bt] and [Opx,Bt] invariant points.

PRESSURE–TEMPERATURE ESTIMATES

The application of conventional thermobarometry to high- and ultrahigh-temperature rocks has its limitations (e.g. Frost & Chacko, 1989; Fitzsimons & Harley, 1994; Raith *et al.*, 1997), but it nevertheless remains a useful tool for comparing the near-peak conditions determined using different petrogenetic grids.

Five sets of associated garnet–orthopyroxene–plagioclase compositions from sapphirine–quartz–garnet–sillimanite ± orthopyroxene granulites (Type A) were used for thermobarometric calibrations. Three were core compositions and two were intermediate to rim compositions. As noted above, garnet cores with sapphirine–quartz inclusions preserve the highest X_{Mg} contents, but the cores of orthopyroxene porphyroblasts associated with garnets are highly aluminous, and have slightly lower X_{Mg} than their rims. Quartz-absent samples were not used for the calibrations because their assemblages formed after the metamorphic peak.

The quartz-bearing Type A granulites contain the near-peak assemblage sapphirine–quartz–orthopyroxene–garnet–sillimanite, with excess quartz in the matrix. Reference temperatures for the pressure calibrations, based on the Al_2O_3 contents of orthopyroxene cores (12·95–11·60 wt %), are 1050–1150°C (Hensen & Harley 1990; Harley 1998*b*; Harley & Motoyoshi, 2000). Such temperatures are consistent with the stability field of the peak assemblages (Grt–Spr–Opx–Qtz ± Pl) in the KFMASH petrogenetic grid. The reference pressures for the temperature calibrations are 11–12 kbar, based on the stability field of the Type A granulite peak assemblage in the same grid.

The garnet–orthopyroxene geobarometers of Wood (1974), Harley & Green (1982), Harley (1984*b*) and Bhattacharya *et al.* (1991) have been used to estimate the peak metamorphic pressure. At a temperature of 1150°C, calibration using the method of Wood (1974) and Harley & Green (1982) yields 11 ± 0·3 and 12·2 ± 0·4 kbar, respectively. The method of Bhattacharya *et al.* (1991) yields a pressure of 8·8 ± 1 kbar for the same temperature. The barometer of Harley (1984*b*) gives a slightly lower value of 8·4 ± 0·6 kbar. Assuming 1050°C, the calculated pressures are lower. The method of Wood (1974) yields 9·0 ± 0·4 kbar, and that of Harley & Green (1982), 8·6 ± 0·2 kbar. The method of Bhattacharya *et al.* (1991) gives 8·2 ± 1·2 kbar, and the experimentally based barometer of Harley (1984*b*), 6·7 ± 0·6 kbar.

Peak temperatures calculated using garnet–orthopyroxene thermometers are considered to be minimum estimates because of extensive Fe–Mg exchange. Assuming a pressure of 12 kbar, the thermometer of Lee & Ganguly (1988) provided the highest reliable average: 1147 ± 17°C. The method of Bhattacharya *et al.* (1991) produced an intermediate value of 1103 ± 13°C, and the method of

Harley (1984*a*), an average of 1042 ± 14°C. The thermometer of Sen & Bhattacharya (1984) yielded the highest temperature: 1274 ± 24°C, and that of Lal (1993), the lowest: 951 ± 21°C. The temperature estimates assuming a pressure of 11 kbar are slightly lower: 1140 ± 17°C by the method of Lee & Ganguly (1988), 1088 ± 13°C by that of Bhattacharya *et al.* (1991) and 1034 ± 14°C by that of Harley (1984*a*). The extreme temperatures estimated using the methods of Sen & Bhattacharya (1984) (1263 ± 24°C) and Lal (1993) (940 ± 20°C) will not be considered further.

We conclude from the above considerations that the near-peak *P–T* conditions were *c.* 1100°C at *c.* 12 kbar. A summary of thermobarometric results based on a temperature normalized to 1150°C and pressure normalized to 12 kbar is given in Table 6.

Orthopyroxene formed at various stages in the metamorphic evolution, so the Al content of orthopyroxene can be used to plot the temperature history. Recent experimental studies of Al solubility in orthopyroxene in the MAS system (Hollis & Harley, 2002) have shown that the Al content of orthopyroxene depends strongly on temperature but weakly on pressure, increasing by about 1 wt % per 26°C. The Al_2O_3 isopleths for orthopyroxene developed from both internally consistent thermodynamic data sets and experimental results (Aranovich & Berman, 1996; Harley, 1998*b*; Harley & Motoyoshi, 2000) can therefore be applied to the granulites considered here.

The resultant evolution path, using the isopleths of Harley & Motoyoshi (2000) in FMAS divariant assemblages, is illustrated in Fig. 10. Temperatures are based on the maximum Al_2O_3 content measured on orthopyroxene in each textural setting. Moraes *et al.* (2002) argued that the temperatures inferred from Al_2O_3 isopleths must be considered maxima because of the presence of minor Fe^{3+} in orthopyroxene. The maximum Al_2O_3 found in the inclusion phases and the cores of orthopyroxene porphyroblasts (up to 12·95 wt %) corresponds to a temperature above 1150°C, and the stability field must be at the higher pressure–temperature side of the [Spl,Bt] point. The Al_2O_3 content of the orthopyroxene porphyroblast rims (up to 9·95 wt %) corresponds to a temperature of *c.* 1050°C and may indicate cooling on the high-pressure side of the [Spl,Bt] invariant point. The orthopyroxene intergrown with sillimanite and quartz preserves a maximum of 8·90 wt % Al_2O_3, and that intergrown with sillimanite only is below 8·80 wt %, both reflecting temperatures above 1000°C. Orthopyroxene in orthopyroxene–cordierite symplectites also has Al_2O_3 contents below 8·20 wt %, corresponding to a temperature just below 1000°C, showing that the decompression path is nearly isothermal. Orthopyroxene in orthopyroxene–sapphirine symplectites has lower Al_2O_3 contents (7·30 wt %) corresponding to temperatures of about 960°C, possibly recording cooling after decompression. Orthopyroxene in orthopyroxene–spinel symplectites, with an Al_2O_3 content of 7·10 wt %, formed at an even lower temperature: 950°C. The orthopyroxene rims on biotite have a maximum of 6·5 wt % Al_2O_3, which indicates a temperature below 950°C during the second decompression stage.

GEOCHRONOLOGY

Type A and Type C granulites from the Highland Complex have been dated by Osanai *et al.* (1996) and Sajeev *et al.* (2003), using the Sm–Nd isochron method.

Type A granulites

Sajeev *et al.* (2003) reported an internal Sm–Nd isochron age for the metamorphism of 1478 ± 58 Ma with an initial ratio of 0·510556 ± 0·000075, based on analyses of a garnet core, whole rock and felsic fraction (quartz + plagioclase). Orthopyroxene plotted off the isochron, probably because several generations of orthopyroxene were present. An orthopyroxene–whole-rock isochron gave a reference age of 550 Ma.

Type C granulites

Osanai *et al.* (1996) reported a Sm–Nd isochron age of *c.* 670 Ma for the metamorphic event based on whole-rock analyses of mafic and sapphirine-bearing granulites (Type C in this study). They also reported a retrograde age of *c.* 430 Ma from a whole-rock–Bt internal isochron.

Other geochronological studies from the Highland Complex

Hölzl *et al.* (1991) concluded from zircon U–Pb analyses that the Highland Complex metabasites were metamorphosed and cooled at about 608 ± 3 Ma. This is possibly the age of peak metamorphism. Pelitic granulites yielded 591 ± 40 Ma using the same method. Kröner *et al.* (1987) reported Pb loss from 3·2–2·4 Ga detrital zircon at *c.* 1·1 Ga, which they speculated might have occurred during an early granulite metamorphic event.

DISCUSSION AND CONCLUSIONS

The *P–T* evolution of the Highland Complex granulites can be divided into four different stages or segments. Segment A consisted of near-isobaric cooling (IBC) at high temperature (above 1100°C). The Al_2O_3 in orthopyroxene isopleths of Harley & Motoyoshi (2000) indicate a temperature of *c.* 1150°C, which might be the maximum attained for this granulite suite. Segment B consisted of near-isothermal decompression (ITD) at high temperature (950–1050°C). Segment C was an

Table 6: Thermobarometric estimations summarized for the coexisting Grt–Opx–Pl pairs in quartz–sillimanite-bearing rocks from the central Highland Complex, Sri Lanka

Garnet		Orthopyroxene		Plagioclase									
X_{Mg}	X_{Grs}	X_{Mg}	X_{Al}	X_{An}	K_D	$P_{(ref)}$	T_{H84}	T_{LG88}	T_{B91}	$T_{(ref)}$	P_{B91}	P_{HG82}	P_{H84}	P_{W74}
0·558	0·022	0·686	0·250	0·286	1·737	12	1056	1167	1118	1150	9·3	11·6	8·7	12·5
0·557	0·012	0·690	0·261	0·299	1·769	12	1039	1140	1099	1150	7·3	11·6	8·8	12·4
0·557	0·022	0·695	0·271	0·290	1·808	12	1028	1135	1092	1150	9·9	11·1	7·7	11·7
0·552	0·020	0·707	0·275	0·266	1·960	12	945	1039	1005	1150	9·0	11·3	6·4	11·9
0·550	0·024	0·709	0·216	0·329	1·986	12	955	1053	1019	1150	9·6	12·7	8·8	13·7

The notations, $T_{(ref)}$ and $P_{(ref)}$ represents reference temperature and pressure, respectively. T_{H84} is used for the temperature resulting from the thermometer of Harley (1984a), whereas T_{LG88} is used for that of Lee & Ganguly (1988) and T_{B91} for that of Bhattacharya *et al.* (1991). P_{B91} represents pressure calibrated using Bhattacharya *et al.* (1991), whereas P_{HG82} is that using Harley & Green (1982), P_{H84} for Harley (1984*b*) and P_{W74} for Wood (1974).

IBC stage involving the formation of biotite and kornerupine at about 7–8 kbar after the growth of multiphase symplectites. Segment D was an ITD stage involving a KFMASH reaction that consumed biotite and produced orthopyroxene.

This is the first evidence for multistage metamorphism to be reported from the pelitic granulites of Sri Lanka. Most previous work implied a 'clockwise' path for both the UHT granulites (e.g. Kriegsman, 1991*b*; Kriegsman & Schumacher, 1999; Osanai *et al.*, 2000) and the medium- to high-temperature granulites (e.g. Hiroi *et al.*, 1994). The work by Schenk *et al.* (1988) on mafic granulites of the Highland Complex yielded a temperature above 900°C from orthopyroxene exsolution in clinopyroxene, which was interpreted as evidence for IBC from higher temperatures.

Our proposed initial near-IBC path (Segment A) is a new concept for the granulites of the Highland Complex. Paths in which the metamorphic peak was reached by a gradual increase of pressure (anticlockwise) are common to many IBC terranes (Warren, 1983; Waters, 1985; Bohlen, 1987; Warren & Hensen, 1989). Such paths have been explained by magmatic accretion (Wells, 1980; Bohlen, 1987). Possibly, the proposed IBC (Segment A) could be a part of an anticlockwise path similar to that proposed for the Napier Complex (e.g. Motoyoshi & Hensen, 1989; Osanai & Yoshimura, 2002). Isobaric heating in the same divariant fields above the [Spl,Bt] invariant point of the KFMASH petrogenetic grid and subsequent cooling after the peak is another possibility. This evolution path is therefore similar to that proposed by Kriegsman & Hensen (1998). Both evolution models are possible, as evidence for the pre-peak assemblages before sapphirine–quartz equilibrium is not preserved, mainly because of the strong overprinting by retrograde reactions.

A near-ITD path on the high-temperature side (Segment B) is required to explain the various symplectites through FMAS continuous reactions. Not all the reactions are observable within one rock type, however, possibly because of the reactions' overstepping. Segment B is similar to Segment A of Harley *et al.* (1990) from Forefinger Point, East Antarctica, in which they suggested the overstepping of reactions during high-temperature decompression. Similar high-temperature overstepping has also been reported from many other UHT terranes (e.g. Brown & Raith, 1996; Mouri *et al.*, 1996; Raith *et al.*, 1997; Harley, 1998*a*; Moraes *et al.*, 2002; Sajeev *et al.*, 2004). It is therefore possible that all reactions described in Segment B could have occurred outside their topological field and thereby become metastable. Droop (1989) first reported such metastable reactions from similar granulites in the Limpopo belt, but the Segment B reactions from the central Highland Complex all involved reactant phases in the matrix, not inclusion phases.

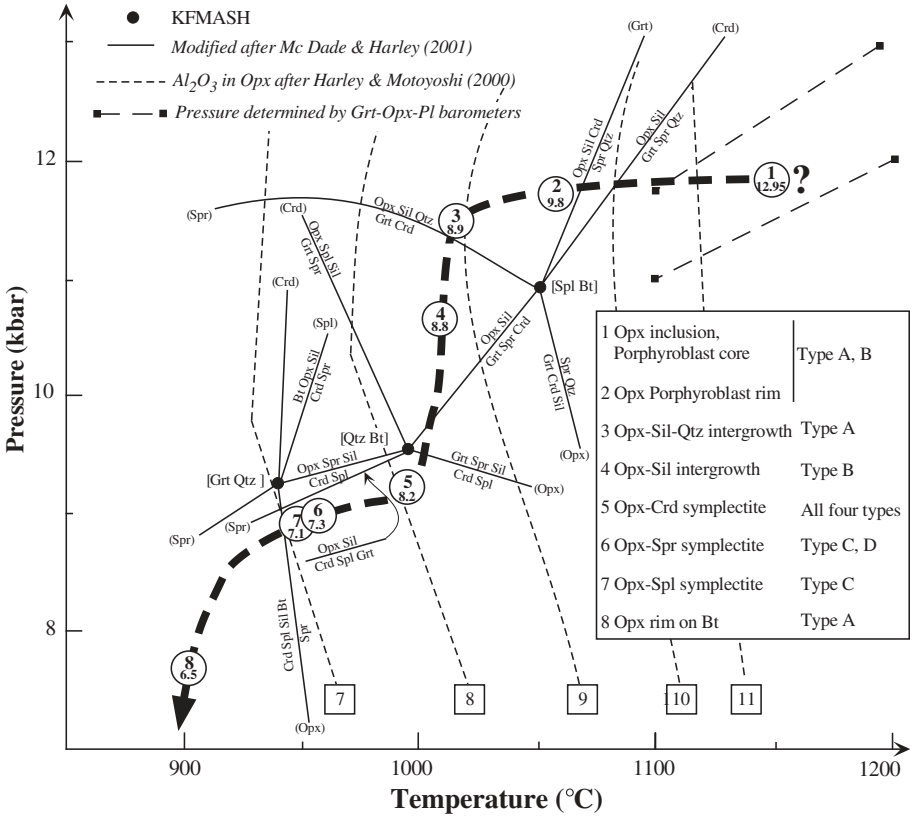

Fig. 10. Interpretation of temperatures derived from the Al_2O_3 in orthopyroxene for each texture (open circles on the evolution path), by using the isopleths of Harley & Motoyoshi (2000) and the petrogenetic grid of McDade & Harley (2001). (See text for further explanation.)

Segment C was a probably a cooling stage that connected two decompression events. The unoriented biotite flakes forming partial rims and intergrowths around other mafic minerals may represent cooling below the [Qtz,Bt] invariant point at 7–8 kbar. A slight variation in pressure is possible within the divariant field below the [Qtz,Bt] and [Grt,Qtz] invariant points. This divariant field has a wide range of stability, but the next stage of near-ITD (Segment D) crosses the KFMASH reaction [reaction (13)] at about 5–5·5 kbar at 750°C, which restricts the field of Segment B above this pressure.

We conclude from this study that the UHT granulites of the Highland Complex probably evolved along an anticlockwise path. There is thereby evidence for both clockwise and anticlockwise evolution trajectories in the same terrane. Harley (1989) and Harley *et al.* (1990) explained the same phenomenon by an extension–magmatic accretion model, involving magmatic underplating and intraplating of thickened crust. Evolution of Segments A and B in the Highland Complex granulites could therefore be an early metamorphic event, and cooling and decompression Segments C and D, a later one.

More geochronological work on the UHT granulites in particular is required to explain the several metamorphic events. From our present results, it is possible that the highest P–T peak metamorphism (12 kbar, 1150°C) occurred at *c.* 1·5 Ga or earlier. The UHT granulites of the Highland Complex can now be correlated petrologically with adjacent UHT terranes such as Forefinger Point, East Antarctica (Harley *et al.*, 1990), Palani Hills (Brown & Raith, 1996; Raith *et al.*, 1997) and the Ganguvarpatti, Madurai block, southern India (Sajeev *et al.*, 2001, 2004), which followed a similar evolution path. Even though these terranes have many petrological features in common, however, any correlation of specific metamorphic events remains uncertain because of the lack of detailed isotope geochronology.

ACKNOWLEDGEMENTS

We are grateful to J. Martignole, J. C. Schumacher and K. K. Podlesskii for their critical and constructive comments. The editor, Kurt Bucher, is thanked for his comments and excellent editorial support. We sincerely thank Ian S. Williams for his constructive comments on the final version of this manuscript. T. Kawakami is acknowledged for help and suggestions. Fieldwork was supported from individual projects led by M. Yoshida and M. Arima (No. 13373005). This work is supported by the Grant-in-Aid

for Scientific Research from the Ministry of Education, Science, Sports and Culture, Japan to Y. Osanai, No. 14340150. This work is a contribution to IGCP 368 and 440.

REFERENCES

Aranovich, L. Ya. & Berman, R. G. (1996). Optimized standard state and solid solution properties of minerals. II. Comparisons, predictions, and applications. *Contributions to Mineralogy and Petrology* **126**, 25–37.

Bhattacharya, A., Krishnakumar, K. R., Raith, M. & Sen, S. K. (1991). An improved set of *A–X* parameters for Fe–Mg–Ca garnets and refinements of the orthopyroxene–garnet thermometer and orthopyroxene–garnet–plagioclase–quartz barometer. *Journal of Petrology* **32**, 629–656.

Bohlen, S. R. (1987). Pressure–temperature–time paths and a tectonic model for the evolution of granulites. *Journal of Geology* **95**, 617–632.

Brown, M. & Raith, M. (1996). First evidence of ultrahigh-temperature decompression from the granulite province of southern India. *Journal of the Geological Society, London* **153**, 819–822.

Carrington, D. P. & Harley, S. L. (1995). Partial melting and phase relations in high-grade metapelites: an experimental petrogenetic grid in the KFMASH system. *Contributions to Mineralogy and Petrology* **120**, 270–291.

Droop, G. T. R. (1989). Reaction history of garnet–sapphirine granulites and conditions of Archaean high-pressure granulite facies metamorphism in Central Limpopo Belt, Zimbabwe. *Journal of Metamorphic Geology* **7**, 383–403.

Droop, G. T. R. & Bucher-Nurminen, K. (1984). Reaction textures and metamorphic evolution of sapphirine-bearing granulites from the Gruf Complex, Italian Central Alps. *Journal of Petrology* **25**, 766–803.

Fitzsimons, I. C. W. & Harley, S. L. (1994). The influence of retrograde cation exchange on granulite *P–T* estimates and a convergence technique for the recovery of peak metamorphic conditions. *Journal of Petrology* **35**, 543–576.

Frost, B. R. & Chacko, T. (1989). The granulite uncertainty principle: limitations on the thermometry in granulites. *Journal of Geology* **97**, 435–450.

Geological Survey Department of Sri Lanka (1982). *Geological Map of Sri Lanka* (8 miles to one inch). Colombo: Geological Survey Department of Sri Lanka. Scale 1:25000, 2 sheets.

Goscombe, B. (1992). Silica-undersaturated sapphirine, spinel and kornerupine granulite facies rocks, NE Strangways Range, Central Australia. *Journal of Metamorphic Geology* **10**, 181–201.

Harley, S. L. (1984*a*). An experimental study of the partitioning of Fe and Mg between garnet and orthopyroxene. *Contributions to Mineralogy and Petrology* **86**, 359–373.

Harley, S. L. (1984*b*). The solubility of alumina in orthopyroxene coexisting with garnet in FeO–MgO–Al_2O_3–SiO_2 and CaO–FeO–MgO–Al_2O_3–SiO_2. *Journal of Petrology* **25**, 665–696.

Harley, S. L. (1989). The origins of granulites: a metamorphic perspective. *Geological Magazine* **126**, 215–247.

Harley, S. L. (1998*a*). Ultrahigh temperature granulite metamorphism (1050°C, 12 kbar) and decompression in garnet (Mg70)–orthopyroxene–sillimanite gneisses from the Rauer Group, East Antarctica. *Journal of Metamorphic Geology* **16**, 541–562.

Harley, S. L. (1998*b*). On the occurrence and characterisation of ultrahigh-temperature crustal metamorphism. In: Treloar, P. J. & O'Brien, P. J (eds) *What Drives Metamorphism and Metamorphic Reactions? Geological Society, London, Special Publications* **138**, 81–107.

Harley, S. L. & Green, D. H. (1982). Garnet–orthopyroxene barometry for granulites and peridotites. *Nature* **300**, 697–701.

Harley, S. L. & Motoyoshi, Y. (2000). Alumina-zoning in orthopyroxene in a sapphirine quartzite: evidence for >1,120°C ultrahigh temperature metamorphism in the Napier Complex, Enderby Land, Antarctica. *Contributions to Mineralogy and Petrology* **138**, 293–307.

Harley, S. L., Hensen, B. J. & Sheraton, J. W. (1990). Two-stage decompression in orthopyroxene–sillimanite granulites from Forefinger point, Enderby Land, Antarctica: implication for the evolution of the Archaean Napier Complex. *Journal of Metamorphic Geology* **8**, 591–613.

Hensen, B. J. (1971). Theoretical phase relations involving cordierite and garnet in the system MgO–FeO–Al_2O_3–SiO_2. *Contributions to Mineralogy and Petrology* **33**, 191–214.

Hensen, B. J. (1986). Theoretical phase relations involving cordierite and garnet revisited: the influence of oxygen fugacity on the stability of sapphirine and spinel in the system Mg–Fe–Al–Si–O. *Contributions to Mineralogy and Petrology* **92**, 362–367.

Hensen, B. J. (1987). *P–T* grids for silica-undersaturated granulites in the systems MAS ($n + 4$) and FMAS ($n + 3$): tools for the derivation of the *P–T* paths of metamorphism. *Journal of Metamorphic Geology* **5**, 255–271.

Hensen, B. J. & Green, D. H. (1973). Experimental study of the stability of cordierite and garnet in pelitic compositions at high-pressure temperatures. III. Synthesis of experimental data and geological applications. *Contributions to Mineralogy and Petrology* **38**, 151–166.

Hensen, B. J. & Harley, S. L. (1990). Graphical analysis of *P–T–X* relations in granulite facies metapelites. In: Ashworth, J. R & Brown, M. (eds) *High-temperature Metamorphism and Crustal Anatexis. Mineralogical Society of Great Britain and Ireland Series* **2**, 19–56.

Hiroi, Y., Ogo, Y. & Namba, L. (1994). Evidence for prograde metamorphic evolution of Sri Lankan pelitic granulites, and implications for the development of continental crust. *Precambrian Research* **66**, 245–263.

Hollis, J. A. & Harley, S. L. (2002). Alumina solubility in orthopyroxene coexisting with sapphirine and quartz. *Contributions to Mineralogy and Petrology* **144**, 473–483.

Hölzl, S., Köhler, H., Kröner, A. & Liew, T. C. (1991). Geochronology of the Sri Lankan basement. In: Kröner, A. (ed.) *The Crystalline Crust of Sri Lanka, Part I. Summary of Research of the German–Sri Lankan Consortium. Geological Survey Department, Sri Lanka, Professional Paper* **5**, 237–257.

Kretz, R. (1983). Symbols of rock-forming minerals. *American Mineralogist* **68**, 277–279.

Kriegsman, L. M. (1991*a*). Structural geology of the Sri Lankan basement: a preliminary review. In: Kröner, A. (ed.) *The Crystalline Crust of Sri Lanka, Part 1. Summary of Research of the German–Sri Lankan Consortium. Geological Survey Department, Sri Lanka, Professional Paper* **5**, 52–68.

Kriegsman, L. M. (1991*b*). Sapphirine-bearing granulites from central Sri Lanka—outcrop description and mineral chemistry. In: Kröner, A. (ed.) *The Crystalline Crust of Sri Lanka, Part 1. Summary of Research of the German–Sri Lankan Consortium. Geological Survey Department, Sri Lanka, Professional Paper* **5**, 178–187.

Kriegsman, L. M. & Hensen, B. J. (1998). Back reaction between restite and melt: implications for geothermobarometry and pressure–temperature paths. *Geology* **26**, 1111–1114.

Kriegsman, L. M. & Schumacher, J. C. (1999). Petrology of sapphirine-bearing and associated granulites from central Sri Lanka. *Journal of Petrology* **40**, 1211–1239.

Kröner, A., Williams, I. S., Compston, W., Baur, N., Vintage, P. W. & Perera, L. R. K. (1987). Zircon ion microprobe dating of high-grade rocks of Sri Lanka. *Journal of Geology* **95**, 775–795.

Kröner, A., Cooray, P. G. & Vintage, P. W. (1991). Lithotectonic subdivision of the Precambrian basement in Sri Lanka. In: Kröner, A. (ed.) *The Crystalline Crust of Sri Lanka, Part I. Summary of Research of the German–Sri Lankan Consortium. Geological Survey Department, Sri Lanka, Professional Paper* **5**, 5–21.

Lal, R. K. (1993). Internally consistent recalibrations of mineral equilibria for geothermobarometry involving garnet–orthopyroxene–plagioclase–quartz assemblages and their application to the South Indian granulites. *Journal of Metamorphic Geology* **11**, 855–866.

Lee, H. Y. & Ganguly, J. (1988). Equilibrium compositions of coexisting garnet and orthopyroxene: experimental determination in the system FeO–MgO–Al_2O_3–SiO_2 and applications. *Journal of Petrology* **29**, 93–113.

Martignole, J. & Martelat, J.-E. (2003).Regional-scale Grenvillian-age UHT metamorphism in the Mollendo–Camana block (basement of the Peruvian Andes). *Journal of Metamorphic Geology* **21**, 99–120.

McDade, P. & Harley, S. L. (2001). A petrogenetic grid for aluminous granulite facies metapelites in the KFMASH system. *Journal of Metamorphic Geology* **19**, 45–59.

Milisenda, C. C., Liew, T. C., Hofmann, A. W. & Kröner, A. (1988). Isotopic mapping of age provinces in Precambrian high-grade terranes: Sri Lanka. *Journal of Geology* **96**, 608–615.

Moraes, R., Brown, M., Fuck, R. A., Camargo, M. A. & Lima, T. M. (2002). Characterization and *P–T* evolution of melt-bearing ultrahigh-temperature granulites: an example from the Anápolis–Itauçu Complex of the Brasília Fold Belt, Brazil. *Journal of Petrology* **43**, 1673–1705.

Motoyoshi, Y. & Hensen, B. J. (1989). Sapphirine–quartz–orthopyroxene after cordierite in the Archaean Napier Complex, Antarctica: evidence for counterclockwise *P–T* path? *European Journal of Mineralogy* **1**, 467–471.

Mouri, H., Guiraud, M. & Hensen, B. J. (1996). Petrology of phlogopite–sapphirine-bearing Al–Mg granulites from Lhouhaouene, In Ouzzal, Hoggar, Algeria: an example of phlogopite stability at high temperature. *Journal of Metamorphic Geology* **14**, 725–738.

Osanai, Y. (1989). A preliminary report on sapphirine/kornerupine granulite from Highland Series, Sri Lanka (extended abstract). *Seminar on Recent Advantages in Precambrian Geology of Sri Lanka, IFS Kandy*.

Osanai, Y. & Yoshimura, Y. (2002). High-temperature limit of crustal metamorphism: a perspective of ultrahigh-temperature metamorphism (in Japanese). *Chishitsu News* **573**, 10–26.

Osanai, Y., Owada, M., Kagami, H., Hamamoto, T. & Hensen, B. J. (1996). Sapphirine granulite and related high *P–T* metamorphic rocks from Highland Complex, Sri Lanka. *Gondwana Research Group Miscellaneous Publication* **4**, 107–108.

Osanai, Y., Ando, K. T., Miyashita, Y., Kusachi, I., Yamasaki, T., Doyama, D., Prame, W. K. B. N., Jayatilake, S. & Mathavan, V. (2000). Geological field work in the southwestern and central parts of the Highland Complex, Sri Lanka during 1998–1999, special reference to the highest grade metamorphic rocks. *Journal of Geoscience, Osaka City University* **43**, 227–247.

Osanai, Y., Sajeev, K., Owada, M., Kehelpannala, K. V. W., Prame, W. K. B. N. & Nakano, N. (2003). Evolution of highest-grade metamorphic rocks from Central Highland Complex, Sri Lanka. *Geological Survey and Mines Bureau, Sri Lanka, Centenary Publication*, 25–31.

Prame, W. K. B. N. (1991). Petrology of Kataragama Complex, Sri Lanka: evidence for high *P–T* granulite facies metamorphism and subsequent isobaric cooling. In: Kröner, A. (ed.) *The Crystalline Crust of Sri Lanka, Part I. Summary of Research of the German–Sri Lankan Consortium. Geological Survey Department, Sri Lanka, Professional Paper* **5**, 200–224.

Raase, P. & Schenk, V. (1994). Petrology of granulite facies metapelites of the Highland Complex Sri Lanka: implication for the metamorphic zonation and the *P–T* path. *Precambrian Research* **66**, 265–294.

Raith, M., Karmakar, S. & Brown, M. (1997). Ultra-high-temperature metamorphism and multi-stage decompressional evolution of sapphirine granulites from the Palni hill ranges, southern India. *Journal of Metamorphic Geology* **15**, 379–399.

Sajeev, K. (2003). Evolution and metamorphic zoning of Highland Complex, Sri Lanka: a comparison with Madurai block, southern India. Ph.D. thesis, Okayama University, 388 pp.

Sajeev, K. & Osanai, Y. (2002). Evidence for counter clockwise evolution of Spr–Qtz & Opx–Sil–Qtz bearing granulites from Highland Complex, Sri Lanka. *16th AGC Geoscience 2002: Expanding Horizons Abstract Volume* **67**, 232.

Sajeev, K. & Osanai, Y. (2003). First finding of osumilite from Highland Complex, Sri Lanka: a case of melt restite interaction resulted isobaric cooling after UHT metamorphism. *Vth Hutton Symposium Abstracts*, 127.

Sajeev, K., Osanai, Y. & Santosh, M. (2001). Ultrahigh-temperature stability of sapphirine and kornerupine in Ganguvarpatti granulite, Madurai Block, Southern India. *Gondwana Research* **4**, 762–766.

Sajeev, K., Osanai, Y., Suzuki, S. & Kagami, H. (2003). Geochronological evidence for multistage-metamorphic events in ultrahigh-temperature granulites from central Highland Complex, Sri Lanka. *Polar Geosciences* **16**, 137–148.

Sajeev, K., Osanai, Y. & Santosh, M. (2004). Ultrahigh-temperature metamorphism followed by two-stage decompression of garnet–orthopyroxene–sillimanite granulites from Ganguvarpatti, Madurai block, southern India. *Contributions to Mineralogy and Petrology* DOI: 10.1007/s00410-004-0592-0.

Schenk, V., Raase, P. & Schumacher, R. (1988). Very high temperature and isobaric cooling before tectonic uplift in the Highland Series of Sri Lanka. *Terra Cognita* **8**, 265.

Schumacher, R. & Faulhaber, S. (1994). Summary and discussion of *P–T* estimates from garnet–pyroxene–plagioclase–quartz-bearing granulite-facies rocks from Sri Lanka. *Precambrian Research* **66**, 295–308.

Seifert, F. (1975). Boron-free kornerupine: a high-pressure phase. *American Journal of Science* **275**, 57–87.

Sen, S. K. & Bhattacharya, A. (1984). An orthopyroxene–garnet thermometer and its application to the Madras charnockites. *Contributions to Mineralogy and Petrology* **88**, 64–71.

Warren, R. G. (1983). Prograde and retrograde sapphirine in metamorphic rocks of Central Arunta Block, Central Australia. *BMR Journal of Australian Geology and Geophysics* **8**, 139–145.

Warren, R. G. & Hensen, B. J. (1989). The *P–T* evolution of the Proterozoic Arunta Block, central Australia, and implications for tectonic evolution. In: Daly, J. S., Cliff, R. A. & Yadley, B. W. D. (eds) *Evolution of Metamorphic Belts. Geological Society, London, Special Publications* **43**, 349–335.

Waters, D. J. (1985). Metamorphic zonation and thermal history of pelitic gneisses from Western Namaqualand, South Africa. *Transactions of the Geological Society of South Africa* **88**, 323–353.

Wells, P. R. A. (1980). Thermal models for magmatic accretion and subsequent metamorphism of continental crust. *Earth and Planetary Science Letters* **46**, 253–265.

Wood, B. J. (1974). The solubility of orthopyroxene coexisting with garnet. *Contributions to Mineralogy and Petrology* **46**, 1–15.